Manuscript Details

Manuscript number	ATMOSRES_2018_890_R1
Title	Weekly Cycle Assessment of PM Mass Concentrations and Sources, and Impacts on Temperature and Wind Speed in Southern Italy
Article type	Research Paper

Abstract

A methodology to detect the weekly cycle impact of the particulate matter (PM), and PM sources on the near surface temperature and wind speed is discussed in the paper. Chemically-speciated PM10 and PM2.5 samples are analyzed to detect the weekly cycle of both the PM mass concentrations and the PM sources identified by the Positive Matrix Factorization technique. The average percent departure (APD) of the PM mass concentration from the mean value calculated for each day of the week shows that a positive (higher values during midweek) and a negative (higher values during weekend) weekly cycle characterizes the PM10 and PM2.5 mass concentrations in Autumn-Winter (AW, September-February) and Spring-Summer (SS, March-August), respectively. The westerly transport of pollution seems to have a role on the negative PM weekly cycle found in SS. The analysis of the six identified aerosol sources indicates that in SS, the mixed anthropogenic and the reacted dust sources likely impact the PM10 negative weekly cycle and that the mixed anthropogenic source likely impacts the PM2.5 negative weekly cycle. The mixed anthropogenic and soil dust sources likely affect in AW the positive weekly cycle of the PM10 mass concentration. Both sources in addition to the reacted dust source seem to affect the PM2.5 mass concentration in AW. The APD analysis of the temperature (T) and wind speed (WS) at the surface from measurements co-located in space and time with the PM ones reveals that the WS and T values are characterized by a negative weekly cycle in AW. Conversely, in SS, the WS-APD value decreases on Sunday and the T-APD values increase in the second half of the week. These last results likely give evidence of the PM impact on the near-surface temperature and wind speed at the study site.

Keywords	weekly cycles; PM mass concentration; temperature and wind speed; Positive Matrix Factorization; long-range transport.
Manuscript category	Aerosol particles

Corresponding Author	Salvatore Romano
Corresponding Author's Institution	University of Salento
Order of Authors	Maria Rita Perrone, Roberta Vecchi, Salvatore Romano, Silvia Becagli, Rita Traversi, Fabio Paladini
Suggested reviewers	Dominique Baumer, A. K. Georgoulias, Daoyi Gong, Camilla Weum Stjern, Mark Jacobson

Submission Files Included in this PDF

File Name [File Type]

COVER LETTER paper weekly cycle.docx [Cover Letter]

Answer to Reviewer 1 (paper weekly cycle).docx [Response to Reviewers]

Answer to Reviewer 2 (paper weekly cycle).docx [Response to Reviewers]

HIGHLIGHTS paper weekly cycle.docx [Highlights]

GRAPHICAL ABSTRACT paper weekly cycle.docx [Graphical Abstract]

revised FINAL MANUSCRIPT paper Weekly Cycle.docx [Manuscript File]

revised SUPPLEMENTARY MATERIAL paper weekly cycle.docx [Supporting File]

marked copy FINAL MANUSCRIPT paper Weekly Cycle.docx [Supporting File]

To view all the submission files, including those not included in the PDF, click on the manuscript title on your EVISE Homepage, then click 'Download zip file'.

Research Data Related to this Submission

There are no linked research data sets for this submission. The following reason is given:
Data will be made available on request

Highlights

"Weekly Cycle Assessment of PM Mass Concentrations and Sources, and Impacts on Temperature and Wind Speed in Southern Italy" by M.R. Perrone et al.

- Weekly cycles of PM10 and PM2.5 mass concentrations and seasonal dependence
- Weekly cycles of temperature and wind speed at the surface and seasonal dependence
- Chemical speciation of PM10 and PM2.5 samples
- Aerosol source identification by Positive Matrix Factorization
- Aerosol source impact on the weekly cycles of PM10 and PM2.5 mass concentrations

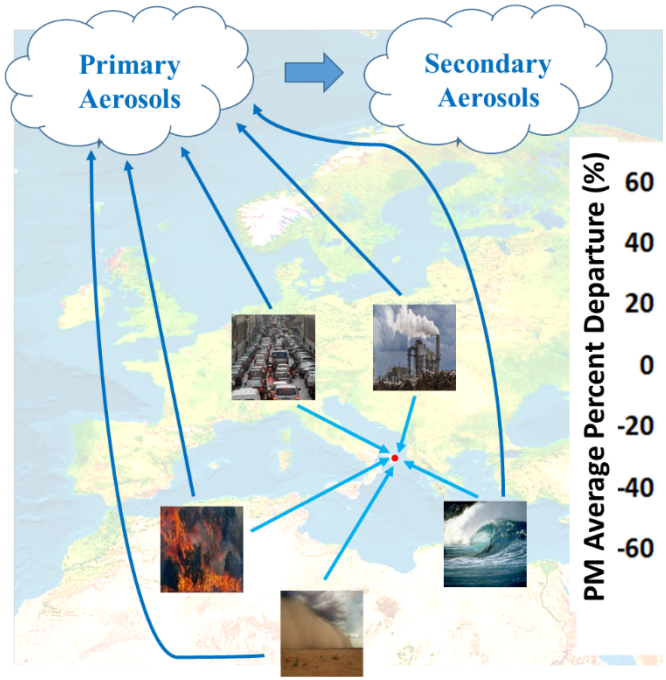
Primary Aerosols
Secondary Aerosols

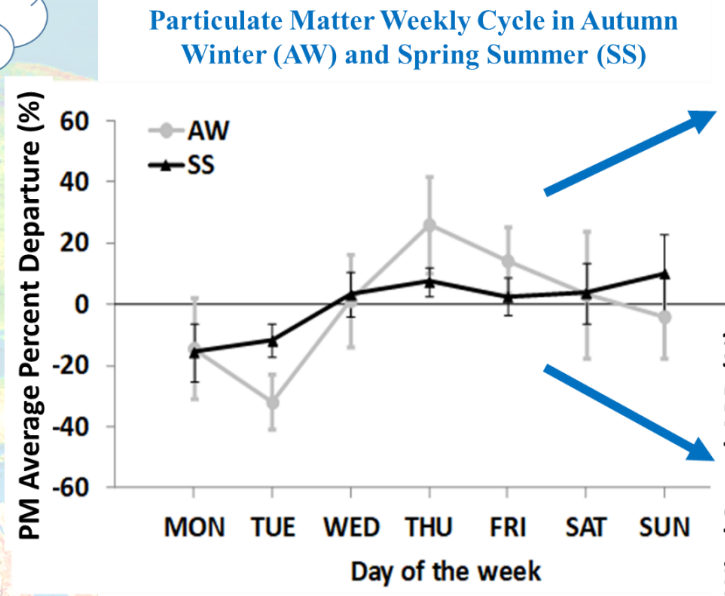
Particulate Matter Weekly Cycle in Autumn Winter (AW) and Spring Summer (SS)
PM Average Percent Departure (%)
60
40
20
0
-20
-40
-60
AW
SS
MON TUE WED THU FRI SAT SUN
Day of the week

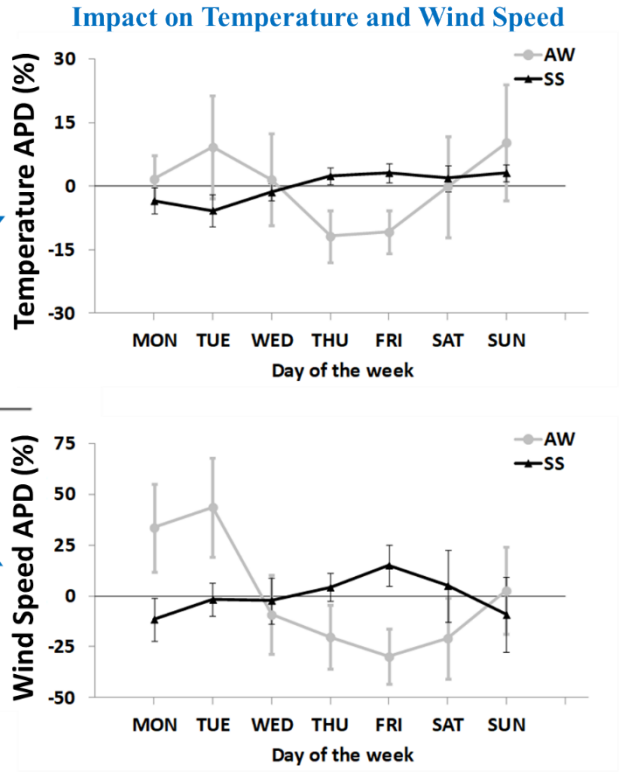
Impact on Temperature and Wind Speed
Temperature APD (%)
30
15
0
-15
-30
AW
SS
MON TUE WED THU FRI SAT SUN
Day of the week
Wind Speed APD (%)
75
50
25
0
-25
-50
AW
SS
MON TUE WED THU FRI SAT SUN
Day of the week

Weekly Cycle Assessment of PM Mass Concentrations and Sources, and Impacts on Temperature and Wind Speed in Southern Italy

Maria Rita Perrone[1], Roberta Vecchi[2], Salvatore Romano[1], Silvia Becagli[3], Rita Traversi[3], Fabio Paladini[1]

[1]Department of Mathematics and Physics, University of Salento,
Via per Arnesano, 73100 Lecce, Italy
[2]Department of Physics, Università degli Studi di Milano, & INFN-Milan
Via Celoria 16, 20133 Milano, Italy
[3]Department of Chemistry, University of Florence,
Via della Lastruccia 3, 50019 Sesto Fiorentino (Florence), Italy

Abstract

A methodology to detect the weekly cycle impact of the particulate matter (PM), and PM sources on the near surface temperature and wind speed is discussed in the paper. Chemically-speciated PM10 and PM2.5 samples are analyzed to detect the weekly cycle of both the PM mass concentrations and the PM sources identified by the Positive Matrix Factorization technique. The average percent departure (APD) of the PM mass concentration from the mean value calculated for each day of the week shows that a positive (higher values during midweek) and a negative (higher values during weekend) weekly cycle characterizes the PM10 and PM2.5 mass concentrations in Autumn-Winter (AW, September-February) and Spring-Summer (SS, March-August), respectively. The westerly transport of pollution seems to have a role on the negative PM weekly cycle found in SS. The analysis of the six identified aerosol sources indicates that in SS, the mixed anthropogenic and the reacted dust sources likely impact the PM10 negative weekly cycle and that the mixed anthropogenic source likely impacts the PM2.5 negative weekly cycle. The mixed anthropogenic and soil dust sources likely affect in AW the positive

weekly cycle of the PM10 mass concentration. Both sources in addition to the reacted dust source seem to affect the PM2.5 mass concentration in AW. The APD analysis of the temperature (T) and wind speed (WS) at the surface from measurements co-located in space and time with the PM ones reveals that the WS and T values are characterized by a negative weekly cycle in AW. Conversely, in SS, the WS-APD value decreases on Sunday and the T-APD values increase in the second half of the week. These last results likely give evidence of the PM impact on the near-surface temperature and wind speed at the study site.

Keywords: weekly cycles; PM mass concentration; temperature and wind speed; Positive Matrix Factorization; long-range transport.

1. Introduction

The impact of the anthropogenic activities on climate is still uncertain based on the Fifth Assessment Report by the International Panel on Climate Change (IPCC, http://www.ipcc.ch/pdf/assessment-report/ar5/wg1/). Weekly cycles in pollution, meteorological, and climate parameters have been investigated to distinguish between anthropogenic and natural contributions to the tested parameters, since no natural processes with a constant cycle of 7 days over long time periods are known to exist (Sanchez-Lorenzo et al., 2008; 2012). Consequently, the existence of weekly cycles in aerosols and meteorological parameters would imply that the human activities affect the Earth's climate even in such short timescales.

Studies of weekly cycles in meteorological parameters have determined contrasting results (Schultz et al., 2007; Rosenfeld et al., 2008; Hendricks Franssen, 2008; Barmet et al., 2009; Quaas et al., 2009). The aerosol-to-precipitation link is non-linear and contains potentially cancelling mechanisms, challenging the discovery of an aerosol signal in meteorological data, according to Stjern (2011). Jacobson and Kaufman (2006) have found that aerosol particles, directly and through their enhancement of clouds, might reduce near-surface wind speeds below them by up to 8% locally. Gong et al. (2007) have investigated the weekly cycle of aerosol concentrations and meteorological parameters in major urban regions over east China, one of the most polluted areas in the world, during summertime in the 2001-2006 years. The PM10 mass concentrations at 29 monitoring stations showed significant weekly cycles with the largest values around midweek and the smallest values in weekend. The meteorological variables also showed notable and consistent weekly cycles. Changes in the atmospheric circulation have likely been triggered by the accumulation of PM10 through diabatic heating of the lower troposphere, based on Gong et al. (2007). Sanchez-Lorenzo et al. (2012) have reported a review on the assessment of large-scale weekly cycles in meteorological variables. They have reviewed the studies reporting significant and non-significant weekly cycles in different meteorological variables over large-scale for different regions around the world and have shown that the assessment of the statistical significance of the weekly cycle faces a number of challenges. The direct and indirect aerosol effects

have been considered possible causes for large-scale weekly cycles because a large-scale weekly cycle in the anthropogenic aerosol emissions was found. In fact, using satellite data, Georgoulias et al. (2015) have found in summer that the total cloud cover (TCC) weekly variability exhibits a very good agreement with the aerosol optical thickness (AOT) weekly variability over Central, Southwestern, and Northeastern Europe and a moderate agreement for Central Mediterranean data. They have suggested that the common weekly variability of TCC and AOT over Europe could be a sign of the aerosol cloud lifetime-effect and the storm invigoration effect giving evidence that the aerosol indirect effects were partially responsible for the correlation between TCC and AOT data.

Weekly cycles in measurements of atmospheric air pollution have been observed in many regions of the world (e.g., Barmet et al., 2009; Srimuruganandam et al., 2010; Liu et al., 2016), with their phase and magnitude greatly dependent on region/sites and seasons. Barmpadimos et al. (2011) have investigated the existence of a weekly cycle for the coarse mass concentration (PM10-PM2.5) monitored at seven sites of the Swiss National Air Pollution Monitoring Network. They have detected a strong weekly variation at the urban street, urban background, and suburban sites, where the maximum day-of-the-week average concentration was larger than the minimum by a factor 1.53. A low-altitude rural background site had a weaker but clear weekly cycle too. Traffic emissions have mainly been considered responsible for the (PM10-PM2.5) weekly cycle. The PM weekly cycle in the USA was also pronounced in urban areas, where weekend concentrations were about 15% lower than the weekday levels, but the differences between weekend and weekdays PM mass concentrations have not been observed at non-urban stations, based on Stern (1977). Bigi and Ghermandi (2016 and references therein) have analyzed time series 7 or 10 years-long to assess the variability of the PM10 and PM2.5 mass concentrations across the Po Valley. They have found a significant weekly cycle (possibly forced by anthropogenic emissions) for several PM2.5 series. The periodicity occurred more often in summer, probably because of the lower contribution to PM by biomass burning emission compounds and secondary inorganic aerosol (especially nitrates) during warmer months (Vecchi et al., 2009; 2018),

88 along with an increase of the primary particle fraction. For all (PM10-PM2.5) series, a significant
89 weekly cycle was found throughout the year.
90 Bäumer et al. (2008) have analyzed the aerosol optical thickness at 440 nm retrieved from sun/sky
91 photometer measurements performed at 14 Central Europe stations operating within the AErosol
92 ROBotic NETwork (AERONET). In 12 out of 14 stations, they have observed that the AOTs showed a
93 weekly periodicity with lower values on Sunday and Monday, but higher values from Wednesday until
94 Saturday. The observed differences were significant at least on a 90% confidence level. Georgoulias
95 and Kourtidis (2011) have investigated over Europe the spatial and temporal variability of the aerosol
96 weekly cycle using the AOTs retrieved from the Terra MODIS (February 2000 - February 2009) and
97 Aqua MODIS (July 2002 - December 2008) satellite measurements. A strong positive (higher values
98 during midweek) weekly cycle appeared over Central Europe (CE), while a strong negative (higher
99 values during weekend) weekly cycle appeared over the North-Eastern Europe. The Central
100 Mediterranean (CM), Eastern Mediterranean (EM), and Central-Eastern Europe (CEE) presented a
101 weak negative weekly cycle. In general, CM, EM, and CEE exhibited different weekly variability for
102 different seasons. The AOT weekly variability examined in conjunction with the dominating synoptic
103 wind pattern showed that the negative AOT weekly cycle over Eastern Europe and the Mediterranean
104 Sea could be partially attributed to the westerly transport of pollution. More specifically, Georgoulias
105 and Kourtidis (2011) showed that air masses from regions with strong weekly cycles (e.g., CE) could
106 significantly affect the aerosol weekly variability over regions away from highly populated and
107 industrialized areas or characterized by a weak weekly cycle. A high-resolution satellite view of the
108 aerosol weekly cycle variability over Central Europe by Georgoulias and Kourtidis (2012) showed that
109 the positive weekly cycle plume was stronger and larger during summer. The day of the maximum
110 average percent departure (APD) ranged between Wednesday-Thursday-Friday becoming Saturday for
111 the Eastern regions and the day of minimum was Monday for Central areas and it became Tuesday
112 moving toward East. The one-day- shift of the day of maximum and minimum for regions situated in

113 Central and Eastern Central Europe was an indication of the aerosol transport due to the dominating
114 westerly wind flow, according to Georgoulias and Kourtidis (2012).
115 The columnar aerosol parameters from sun/sky photometer measurements and near-surface aerosol
116 parameters from nephelometer measurements were used by Perrone et al. (2015) to investigate the
117 aerosol weekly cycle at the monitoring site of this study, in the Central Mediterranean. The daily
118 evolution of the aerosol properties referring to working days (Monday to Friday) and Sunday and the
119 weekly cycle analysis suggested that the aerosol source contributions varied during the weekends. In
120 particular, the yearly-averaged ground-level and columnar aerosol parameters indicated that the
121 weekend daily means of the aerosol optical depth and scattering coefficient were likely affected by the
122 transboundary pollution from Eastern Europe, due to weekday anthropogenic activities, in agreement
123 with the results by Georgoulias and Kourtidis (2011).
124 Mass concentrations of the simultaneously collected PM2.5 and PM10 samples are analyzed in this
125 study, with the main aim of investigating the existence of a weekly cycle and contributing to the
126 understanding of the results reported by Perrone et al. (2015). The PM sampling was performed from
127 October 2014 to October 2015 at a coastal site of southeastern Italy, in the Central Mediterranean Basin.
128 The chemical composition of the collected PM2.5 and PM10 samples is analyzed and the Positive
129 Matrix Factorization (PMF) technique (Paatero and Tapper, 1994) is applied to the chemically speciated
130 PM10 and PM2.5 samples to determine the main pollution sources at the study site and their potential
131 impacts on the weekly cycle of PM2.5 and PM10 mass concentrations. The weekly cycle in nitrogen
132 dioxide (NO_2) measurements, co-located in space and time with the PM measurements, is also analyzed.
133 NO_2 is a relevant air pollutant due to combustion sources and contributes to the formation of nitrate
134 aerosols by gas-to-particle conversion processes (Seinfeld and Pandis, 1998). The weekly cycle in
135 temperature and wind speed measurements, co-located in space and time with the PM measurements,
136 is also analyzed to investigate their relationships with the PM weekly cycle. It is noteworthy that it is
137 beyond the scope of the paper to find cause-effects relationships. As outlined by Sanchez-Lorenzo et al.
138 (2012) and more recently by Georgoulias et al. (2015), it has been established that the aerosol's effects

have a clear impact on the energy balance, and especially on precipitation processes and clouds, temperature and wind speed. However, more research is needed to identify, understand, and quantify the physical mechanisms beyond the observed atmospheric changes. Therefore, one of the main aims of this paper is to contribute to the understanding of the aerosol-meteorology feedback by analysing co-located in space and time surface measurements of chemically speciated PM10 and PM2.5 particles, NO_2, temperature, and wind speed. Most of the previous studies based on surface measurements have mainly analyzed long-time series of PM mass concentrations (e.g., Bigi and Ghermandi, 2016).

2. Sampling site and methods

2.1 Site description and sampling instrument

The PM samples have been collected at ~10 m above the ground level, at the Mathematics and Physics Department of the University of Salento. The monitoring site is in a suburban area (40.4°N; 18.1°E), ~6 km away from the city center of Lecce, ~20 km away from both the Ionian and Adriatic seas, and ~100 and 800 km away from the Balkan and North African coasts, respectively (Figure 1). Consequently, it can be considered representative of coastal sites of the Central Mediterranean (Perrone et al., 2013) affected by long-range-transported pollution from surrounding countries (Perrone et al., 2015).

A low volume (2.3 $m^3 h^{-1}$) HYDRA-FAI dual sampler was used to simultaneously collect 24-hour PM10 and PM2.5 samples on 47-mm-diameter pre-heated filters (PALLFLEX, Tissuquartz) from October 2014 to October 2015. The sampling was made on 7 consecutive days (from Monday to Sunday) of each month and PM samples from 13 different weeks were collected for a total of 90 samples. Filters were conditioned for 48 hours in an air-controlled chamber (25°C and 50% humidity) before and after sampling and the PM mass was determined by gravimetric measurements. Uncertainties on mass concentrations were lower than 5%. The PM loaded filters were divided in four portions for the determination of inorganic ions, metals, organic and elemental carbon.

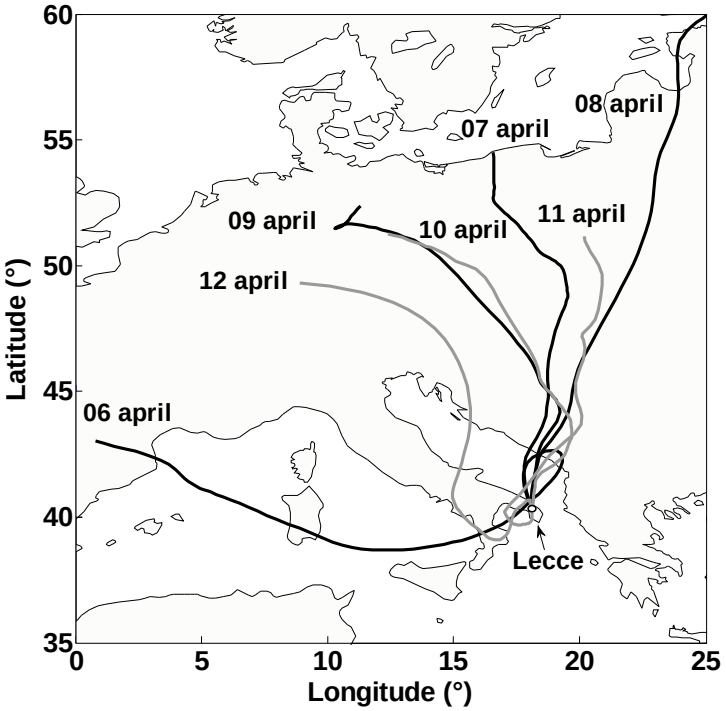

Figure 1. Geographical location of the monitoring site. The open dot indicates the location of the monitoring site at the Mathematics and Physics Department of Salento University, in Lecce (southeastern Italy). Grey and black lines show the pathways of the four-day analytical back trajectories that reached the study site at 500 m above sea level (asl), at 12:00 UTC of each day of the week April 6-12, 2015.

2.2 Chemical analyses

The PM2.5 and PM10 samples were chemically characterized for ions and metals at the Chemistry Department of the University of Florence. Ion chromatography analyses were performed by a Flow Analysis Ion Chromatography (FA-IC, modified after Morganti et al., 2007) for selected anions (Cl^-, NO_3^-, SO_4^{2-}, MS^-) and cations (Na^+, NH_4^+, K^+, Mg^{2+}, Ca^{2+}). Particular attention was devoted to the evaluation of the blanks, which was at least one order of magnitude lower than the mean concentration found in the analyzed samples for each reported ion result. The detection limit was 0.08 ng m^{-3} for Cl^-, NO_3^-, SO_4^{2-}, MS^-, Na^+, NH_4^+, and K^+ and 0.16 ng m^{-3} for Mg^{2+} and Ca^{2+}.

A Varian 720-ES Inductively Coupled Plasma Atomic Emission Spectrometer (ICP-AES) equipped with an ultrasonic nebulizer (U5000 AT^{+}, Cetac Technologies Inc.) was used to determine the mass concentration of selected metals (Al, As, Ba, Cd, Ce, Co, Cr, Cu, Fe, La, Mn, Mo, Ni, P, Pb, Sr, Ti, V, Zn). Elements were extracted by using HNO_3 and H_2O_2 in a macro-wave oven in accordance with the methodology UNI EN 14902 2005. High purity nitric acid obtained by sub-boiling distillation was used in order to reduce blank values. Samples were spiked with 100 ppb of Ge (λ = 209.426 nm) used as internal standard. Calibration standards were prepared by gravimetric serial dilution from mono standards at 1000 mg L^{-1}. Detection limits for Al, As, Ba, Cd, Ce, Co, Cr, Cu, Fe, La, Mn, Mo, Ni, P, Pb, Sr, Ti, V, and Zn were 0.1, 0.2, 0.1, 0.4, 0.05, 0.1, 0.02, 0.13, 0.1, 0.02, 0.04, 0.05, 0.04, 0.2, 0.1, 0.05, 0.03, 0.04, and 0.22 ng m^{-3}, respectively.

More details about ion and metal analyses can be found in Becagli et al. (2012).

The thermal optical transmittance technique by means of the Sunset Carbon Analyzer Instrument (Birch and Cary, 1996) was used to determine the EC and OC mass concentrations in a 1.5 cm^2 punch of the filter sample. The used temperature program follows the NIOSH protocol (NIOSH, 1999; Birch and Cary, 1996). The uncertainties in the EC and OC measurements given by the manufacturer (Sunset Lab, OR) are estimated to be of the order of 5%. The OC and EC analyses were performed at the Mathematics and Physics Department of the University of Salento. More details can be found in Perrone et al. (2009).

2.3 Receptor modelling

The Positive Matrix Factorization (PMF, EPA-PMF v.5.0, Norris et al., 2014) was applied to the PM10 and PM2.5 chemically speciated dataset to retrieve major emission sources impacting on the study area. The PMF is a widespread receptor model (Belis et al., 2014) based on a least squares program solving models where the data values are fitted by sums of products of unknown factor elements (Paatero, 2000). For bilinear problems, it takes the form $X = G \cdot F + E$, where X is the known

n by m matrix of the m measured chemical species in n samples, G is an n by p matrix of factor contributions to the samples, F is a p by m matrix of species concentrations in the factor profile, p is the number of factors. The G and F are factor matrices to be determined and they are constrained only to non-negative values. E is defined as the residual matrix, i.e. the difference between the measurements X and the model Y = G·F as a function of G and F.

The dataset (composed of 90 samples) was analyzed by the EPA-PMF and comprised only strong variables (23 aerosol chemical components plus PM mass in both cases), defined according to the signal-to-noise criterion reported in Paatero (2015). All data were pre-treated according to Polissar et al. (1998) as for uncertainties, below detection limits and missing data.

3. Results and discussion

3.1 PM mass concentrations and weekly cycle

Previous investigations at the study site (e.g., Perrone et al., 2013, 2015; Pietrogrande et al., 2018) have shown that the chemical, optical, and microphysical properties of the ground level PM are season dependent. Consequently, the data of this study are grouped for Autumn-Winter (AW, September-February) and Spring-Summer (SS, March-August) to better detect a weekly cycle and investigate its seasonal dependence. The AW and SS PM samples are representative of 6 and 7 measurement weeks, respectively. Table 1 shows the mean mass concentration of the PM10 and PM2.5 samples for AW and SS. The mean mass concentration of the 41 AW samples and the 49 SS samples shows that 71 and 76% of the PM10 mass, respectively, is accounted for by the PM2.5 particles because of the significant contribution of fine mode particles at this site (Perrone et al., 2009, 2014). In SS, the significant contribution of the photochemical produced species over the Mediterranean Basin combined with the less precipitation contribute to the increase of the mean percentage of the PM2.5 mass. The mean PM10 mass concentration is 34 μg m^{-3} in AW and decreases by 15% in SS. The mean PM2.5 mass concentration, which is 24 μg m^{-3} in AW and decreases by 8% in SS (Table 1),

suggests that nearly 7% of the PM10 decrease is due to the reduction of the coarse mode particle contribution. The mean PM2.5 mass concentration of this study is in good agreement with the one retrieved in PM2.5 samples collected from July 2008 to May 2010 at the same site (Perrone et al., 2013).

The identification of the PM weekly pattern in AW and SS is based on Xia et al. (2008). A new daily index of the PM mass concentration ($PM_{j,m,new}$) corresponding to the day *j* (Monday-Sunday) of the week *m* is calculated from the following equation:

$$PM_{j,m,new} = 100 \cdot (PM_{j,m} - PM_{av,m}) / PM_{av,m} \quad (1)$$

where *j* varies from 1 to 7, *m* ranges from 1 to 13, $PM_{av,m}$ represents the weekly average of PM mass concentration, and $PM_{j,m,new}$ represents the percentage departure of the initial daily value $PM_{j,m}$ from the weekly average ($PM_{av,m}$). The $PM_{j,m,new}$ values are averaged for each day of the week separately and the average percent departure (APD) of the mass concentration is calculated for each day of the week. Figure 2 shows the APD of the (a) PM10 and (b) PM2.5 mass concentrations as a function of the day of the week in AW (grey line) and SS (black lines). Error bars represent the standard error of the mean (SEM). The PM10 and PM2.5 APD values are characterized by a similar weekly cycle in both AW and SS because of the large contribution (>70%) of the PM2.5 particles. A positive (higher values during midweek) weekly cycle characterizes the PM10 and PM2.5 mass concentrations in AW. The Thursday-APD value is approximately 20% higher than the Sunday-APD value in AW and the difference is statistically significant at the 88 and 92% confidence level for PM10 and PM2.5 samples, respectively, based on a two-tailed t-test. A negative (higher values during weekend) weekly cycle characterizes the PM10 and PM2.5 mass concentrations in SS. The Sunday-APD value is about 30% higher than the Monday-APD value in SS and the difference is significant at the 90 and 94% confidence level for PM10 and PM2.5 samples, respectively, based on a two-tailed t-test. These results are consistent with those reported by Georgoulias and Kourtidis (2011) and Perrone et al. (2015). Barmet et al. (2009) have shown that tests between two groups, such as the t-test, may overestimate the significance and therefore they

253 may be inappropriate. They considered more appropriate the Kruskal-Wallis (KW) test since it does not
254 require normality as the t-test and it is also adequate to compare more than two groups. Table 2 provides
255 the confidence level percentage for PM10 and PM2.5 samples calculated by the t-test and the KW-test.
256 Both tests provide similar confidence levels in SS, but the KW-test provides lower confidence levels
257 than the t-test in AW, confirming what was already outlined by Barmet et al. (2009). The confidence
258 level as a percentage from the KW-test are given in brackets in each plot of Figure 2. The higher day-
259 by-day variability of the PM mass concentration in AW than in SS has likely contributed to the
260 confidence level difference of the two tests in AW. As mentioned, Bigi and Ghermandi (2016) have
261 analyzed long time series of PM2.5 mass concentrations at 44 sites across the Po Valley and found that
262 all sites exhibited a significant weekly pattern in summer and almost none in winter, in reasonable
263 accordance with the results of this study. The lower contribution to the PM by secondary inorganic
264 aerosols (especially nitrate and organic matter) and by biomass burning emissions (see e.g. Bernardoni
265 et al., 2011) during warmer months has been considered responsible for the significant weekly cycle
266 observed in summer. Georgoulias and Kourtidis (2012) also showed that the positive weekly cycle
267 plume appearing over Central Europe was stronger and larger during summer.
268

Table 1. The mean mass concentrations and related standard errors of the mean (SEMs) of the analyzed components in PM10 and PM2.5 samples for Autumn-Winter (AW, September-February) and Spring-Summer (SS, March-August). The mean mass percentages of measured species with respect to the total sampled mass are reported in brackets.

Species	PM10 (ng m^{-3})				PM2.5 (ng m^{-3})			
	AW		SS		AW		SS	
	Mean	SEM	Mean	SEM	Mean	SEM	Mean	SEM
Na^+	636 (1.9)	27	718 (2.5)	25	218 (0.9)	10	224 (1.0)	9
NH_4^+	377 (1.1)	19	633 (2.2)	17	450 (1.9)	19	913 (4.2)	17
K^+	452 (1.3)	24	296 (1.0)	22	451 (1.9)	25	296 (1.3)	23
Mg^{2+}	114 (0.3)	3	165 (0.6)	3	40 (0.2)	2	76 (0.3)	1
Ca^{2+}	433 (1.3)	18	807 (2.8)	17	179 (0.7)	7	402 (1.8)	6
Cl^-	465 (1.4)	34	218 (0.8)	31	144 (0.6)	11	66 (0.3)	10
NO_3^-	2170 (6.4)	110	1910 (6.6)	100	1198 (5.0)	80	583 (2.7)	73
SO_4^{2-}	2103 (6.2)	76	4440 (15.3)	70	1920 (8.0)	70	4303 (19.6)	64
MS^-	14 (0.04)	1	45 (0.2)	1	13 (0.05)	1	41 (0.2)	1
Al	101 (0.3)	10	153 (0.5)	9	53 (0.2)	7	89 (0.4)	6
Ba	6.2 (0.02)	0.2	4.7 (0.02)	0.2	3.3 (0.01)	0.1	2.2 (0.01)	0.1
Cd	0.5 (0.002)	0.1	0.1 (0.0003)	0.1	0.41 (0.002)	0.04	0.12 (0.0005)	0.04
Ce	0.17 (0.001)	0.01	0.12 (0.0004)	0.01	0.12 (0.0005)	0.01	0.09 (0.0004)	0.01
Co	0.4 (0.002)	0.1	0.2 (0.0007)	0.1	0.21 (0.0009)	0.01	0.14 (0.0006)	0.01
Cr	1.8 (0.006)	0.1	1.9 (0.007)	0.1	1.4 (0.006)	0.1	1.5 (0.007)	0.1
Cu	10.0 (0.03)	0.4	7.0 (0.02)	0.4	6.3 (0.03)	0.4	3.7 (0.02)	0.4
Fe	255 (0.8)	10	227 (0.8)	9	128 (0.5)	5	119 (0.5)	5
La	0.09 (0.0003)	0.01	0.07 (0.0002)	0.01	0.10 (0.0004)	0.01	0.04 (0.0002)	0.01
Mn	3.6 (0.01)	0.1	4.9 (0.02)	0.1	2.1 (0.009)	0.1	2.8 (0.01)	0.1
Mo	2.8 (0.008)	0.1	2.3 (0.008)	0.1	2.7 (0.01)	0.1	2.3 (0.01)	0.1
Ni	4.1 (0.01)	0.5	3.1 (0.01)	0.5	2.8 (0.01)	0.1	2.9 (0.01)	0.1
P	21.5 (0.06)	0.5	32.9 (0.1)	0.5	14.5 (0.06)	0.3	21.7 (0.1)	0.2
Pb	13 (0.04)	3	8 (0.03)	2	9 (0.04)	1	5 (0.02)	1
Sr	1.7 (0.005)	0.1	1.9 (0.007)	0.1	0.9 (0.004)	0.1	0.9 (0.004)	0.1
Ti	2.8 (0.008)	0.2	4.9 (0.02)	0.2	1.5 (0.006)	0.1	4.1 (0.02)	0.1
V	2.3 (0.007)	0.1	5.3 (0.02)	0.1	2.1 (0.009)	0.1	5.0 (0.02)	0.1
Zn	67 (0.2)	6	49 (0.2)	5	58 (0.2)	5	42 (0.2)	5
OC	8990 (26.4)	380	5040 (17.3)	360	8050 (33.5)	350	4430 (20.1)	320
EC	2980 (8.8)	150	1660 (5.7)	140	2860 (11.9)	150	1580 (7.2)	130
PM	34000	800	29000	5000	24000	800	22000	800

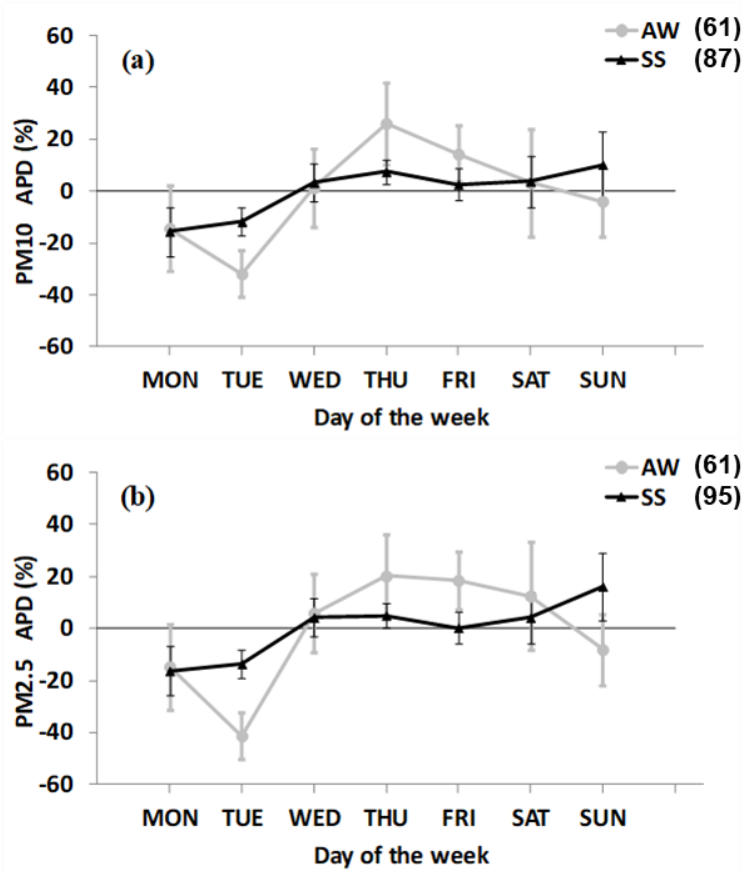

274

275 **Figure 2.** Average Percent Departure (APD) of the (a) PM10 and (b) PM2.5 mass concentrations as a function of the day
276 of the week and for Autumn-Winter (AW, dots and grey line) and Spring-Summer (SS, triangles and black lines). Error
277 bars represent the standard error of the mean (SEM). The confidence level percentage of the difference between the
278 Thursday and the Sunday APD for AW and between the Monday and the Sunday APD for SS by the Kruskal-Wallis test
279 is reported in brackets.

280

281 At the study site, Perrone et al. (2013) have investigated the impact of long-range transport on the
282 PM mass concentration. They found from the cluster analysis of the four-day back trajectories that
283 the airflows from the Northeastern European regions and the Adriatic coast were responsible for the
284 largest median values of the PM2.5 and PM1 mass concentrations. Consequently, the westerly
285 transport of pollution due to weekday anthropogenic activities, favoured in SS by the low air mass
286 renovation occurring over the Mediterranean Basin (Querol et al., 2009), is likely responsible for the
287 negative PM weekly cycle found in SS at the study site, as Georgoulias and Kourtidis (2011) also
288 showed. The Mediterranean Basin is a crossroad of air pollution (Lelieveld et al., 2002) being affected

289 by polluted particles from the industrialized surrounding regions and by desert dust from the African
290 continent. Consequently, Querol et al. (2009) pointed out that most Mediterranean sites face the
291 problem of the long-range transport of PM, which adds to local emissions, preventing to reach air
292 quality objectives set by public authorities.

293

294 **Table 2.** Confidence level percentage for PM10, PM2.5, NO_2, temperature (T), and wind speed (WS) in Autumn-Winter
295 (AW) and in Spring-Summer (SS) calculated by the two-tailed t-test and the Kruskal-Wallis (KW) test. The compared days
296 of the week are also reported in the Table.

Parameter	Season	Compared Days	Confidence Level (%)	
			t-test	KW-test
PM10	AW	Thursday-Sunday	88	61
	SS	Monday-Sunday	90	87
PM2.5	AW	Thursday-Sunday	92	61
	SS	Monday-Sunday	94	95
NO_2	AW	Friday-Sunday	90	87
	SS	Wednesday-Sunday	93	96
T	AW	Thursday-Sunday	82	61
	SS	Tuesday-Sunday	85	96
WS	AW	Tuesday-Friday	96	96
	SS	Monday-Friday	91	87

297

298

299 *3.2 Chemical PM characterization in AW and SS*

300 The mean chemical composition of the PM10 and PM2.5 samples is analyzed to characterize the main
301 pollution sources and investigate their relationships with the observed weekly cycle of mass
302 concentrations (Figure 2a-b). The daily-averaged mass concentrations (± 1 SEM) of the analyzed
303 inorganic ions (Cl^-, Na^+, SO_4^{2-}, NO_3^-, NH_4^+, K^+, Mg^{2+}, Ca^{2+}, MS^-), metals (Al, As, Ba, Cd, Ce, Co,
304 Cr, Cu, Fe, La, Mn, Mo, Ni, P, Pb, Sr, Ti, V, Zn), EC, and OC are in Table 1 for the PM10 and PM2.5
305 samples in AW and SS. The marine- and crust-originated ions (Cl^-, Na^+, Mg^{2+}, and Ca^{2+}) and NO_3^-

306 are the dominant ionic components in the coarse fraction being their mass concentration more than
307 twice greater in PM10 than in PM2.5 samples in AW and SS, respectively. SO_4^{2-}, NH_4^+, K^+, and MS^-
308 are dominant ionic components in the PM2.5 fraction being their mass concentration approximately
309 equal in the PM10 and PM2.5 samples, both in AW and in SS. Particular attention deserves the NH_4^+
310 mass concentration that is 1.2 and 1.4 greater in PM2.5 than in PM10 samples in AW and in SS,
311 respectively. Similar results have been found at western and eastern Mediterranean sites by other
312 authors (e.g., Nicolas et al., 2009; Pey et al., 2009; Koçak et al., 2007). The interaction of ammonium
313 particulate with alkaline PM is responsible for the loss of ammonium (Danalatos and Glavas, 1999).
314 In fact, at the monitoring site of this study, Perrone et al. (2009, 2011, 2016) found that the NH_4^+
315 mass percentage, calculated with respect to the total detected ion mass, decreases as the mass
316 percentage of Na^+, Mg^{2+}, Ca^{2+}, and K^+ increases. Note that the reactions leading to the loss of
317 ammonium particulate are favoured in total suspended particulate and PM10 samples, being Na^+,
318 Mg^{2+}, and Ca^{2+} dominant ions in the coarse fraction.

319 The higher mass contribution of nitrate in PM10 than in PM2.5 samples mainly found in SS is also
320 peculiar of most coastal sites of the southern Mediterranean Basin (Bardouki et al., 2003). It is
321 probably due to the low thermal stability of NH_4NO_3 in SS, when the formation of HNO_3 instead of
322 NH_4NO_3 is favoured under the prevalent warm conditions of most of the Central Mediterranean sites
323 (Querol et al., 2008). The presence of gaseous HNO_3 and the possible interaction of the pollutant with
324 mineral calcium carbonate, K^+, and sea salt may account for the increase of the coarse nitrate
325 proportion (Perrone et al., 2013). The NO_3^- partitioning in the coarse fraction can be quite variable
326 depending on the ability of coarse particles to trap gaseous HNO_3 (e.g., Putaud et al., 2010; Koçak et
327 al., 2007). Fine nitrate particles are usually the result of nitric acid/ammonia reactions leading to the
328 formation of ammonium nitrate.

329 Organic and elemental carbon (OC and EC, respectively) are relevant species in PM10 and PM2.5
330 samples. Their mass concentration is approximately equal in PM10 and PM2.5 samples, both in AW

and in SS, being mostly in the fine mode fraction. OC represents 33 and 20% of the PM2.5 mass in AW and SS, respectively. EC accounts for 12 and 7% of the PM2.5 mass in AW and SS, respectively. Table 1 highlights the significant seasonal dependence of the contributions of the detected species. The mass concentration of Na^+, NH_4^+, Mg^{2+}, Ca^{2+}, SO_4^{2-}, and MS^- is greater in SS than in AW. Conversely, the mass concentration of K^+, NO_3^-, EC, and OC is greater in AW than in SS because of the seasonal dependence of the pollution sources, as it will be shown in the following. The main results of this study on the chemical composition and seasonal dependence of the PM10 and PM2.5 samples are comparable to those reported in previous publications (e.g., Perrone et al., 2009, 2011, 2013), where the PM mass concentration and chemical composition have also been compared with the corresponding ones of different Mediterranean coastal sites.

3.2.1 Weekly cycle of chemical component mass concentrations

The weekly cycles of Na^+, NH_4^+, K^+, Ca^{2+}, NO_3^-, SO_4^{2-}, OC, and EC mass concentrations are analyzed to investigate their respective impact on the weekly cycle of the PM10 and PM2.5 mass concentrations (Figure 2). The above selected chemical components show mass percentages greater than 1% in PM10 and PM2.5 samples, both in AW and in SS. Figure 3 shows the APD values of Na^+, NH_4^+, K^+, and Ca^{2+} mass concentrations in AW (grey) and SS (black), both for the PM10 (a-c-e-g, respectively) and PM2.5 (b-d-f-h, respectively) particles. Analogously, the APD values of NO_3^-, SO_4^{2-}, OC, and EC are shown in Figure 4a-h. A quick look at Figures 3 and 4 highlights that the AW- and SS-APD values of the investigated chemical components are generally characterized by a similar weekly cycle trend in PM10 and PM2.5 samples. The APD and corresponding SEM values are characterized by a lower day-by-day variation in SS than in AW, as the APD values of PM10- and PM2.5-mass concentration also show (Figure 2). The above reported result can be explained by the low frequency of rainy days occurring in SS over the Mediterranean Basin, which favours the air mass aging, enhances natural and anthropogenic dust resuspension and limits the removal of atmospheric particles by wet deposition (Perrone et al., 2015). Note that Perrone and Romano (2018) have shown that the planetary boundary

357 layer (PBL) height is larger in AW than in SS at the study site, and that the daily cycle changes of the
358 PBL height are more relevant in AW than in SS, in contrast to what is generally observed. The level
359 of confidence (%) of the difference between the Sunday and Thursday APD value of each chemical
360 component has been calculated by the KW- and the two-tailed t-test, to better evaluate the weekly
361 cycle significance of the measured PM chemical components. The KW-test confidence levels (%) are
362 provided in brackets in each plot of Figures 3 and 4 for AW and SS. Table S1 in the supplementary
363 material provides the confidence levels (%) calculated from the KW- and the t-test.

364

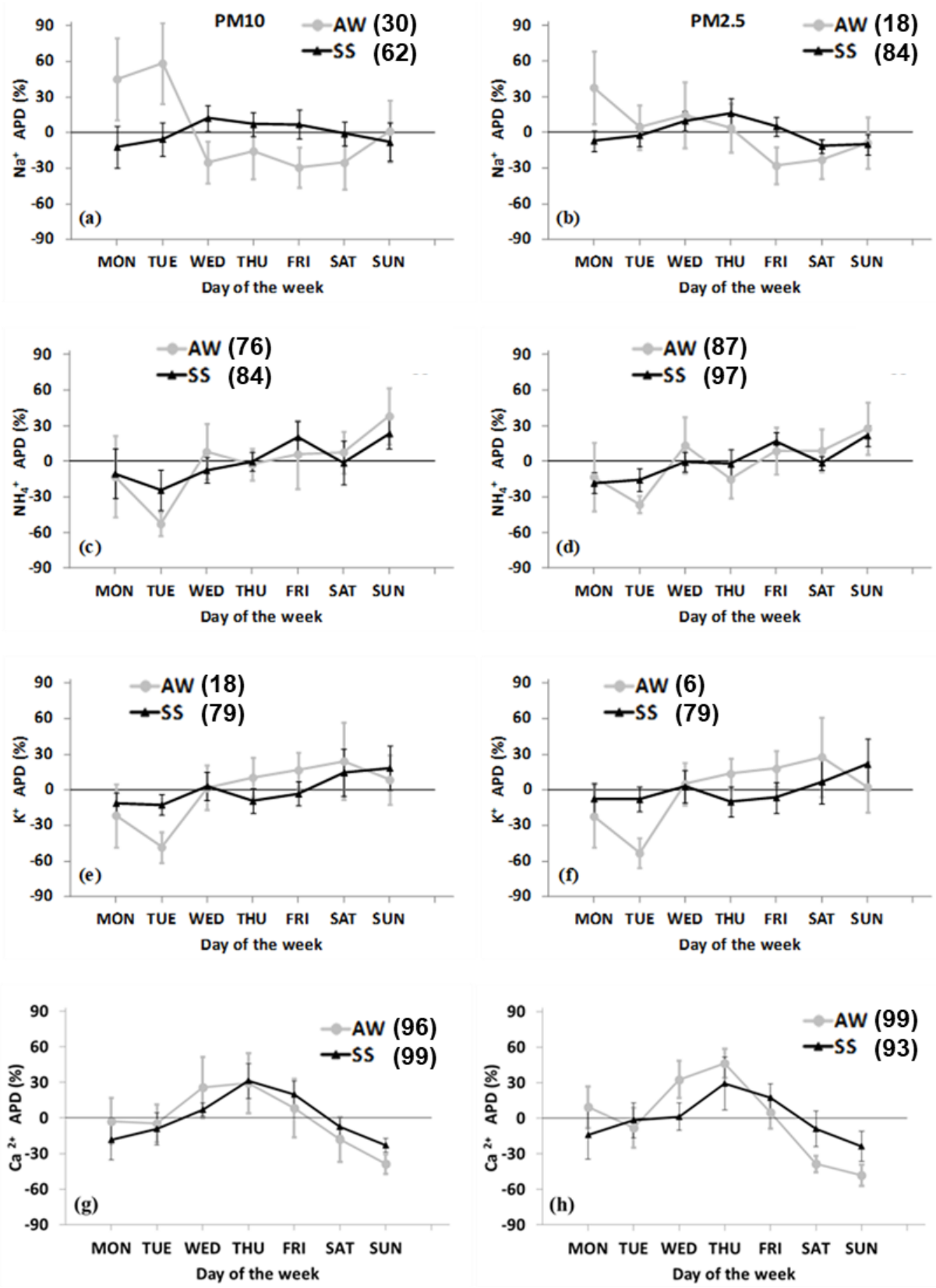

Figure 3. PM10 and PM2.5 Average Percent Departure (APD) of the Na^+ (a and b, respectively), NH_4^+ (c and d, respectively), K^+ (e and f, respectively), and Ca^{2+} (g and h, respectively) mass concentration as a function of the day of the week and for Autumn-Winter (AW, dots and grey line) and Spring-Summer (SS, triangles and black lines). Error bars represent the standard error of the mean (SEM). The confidence level percentage value of the difference between the Thursday and the Sunday APD for each chemical compound by the Kruskal-Wallis test is reported in brackets.

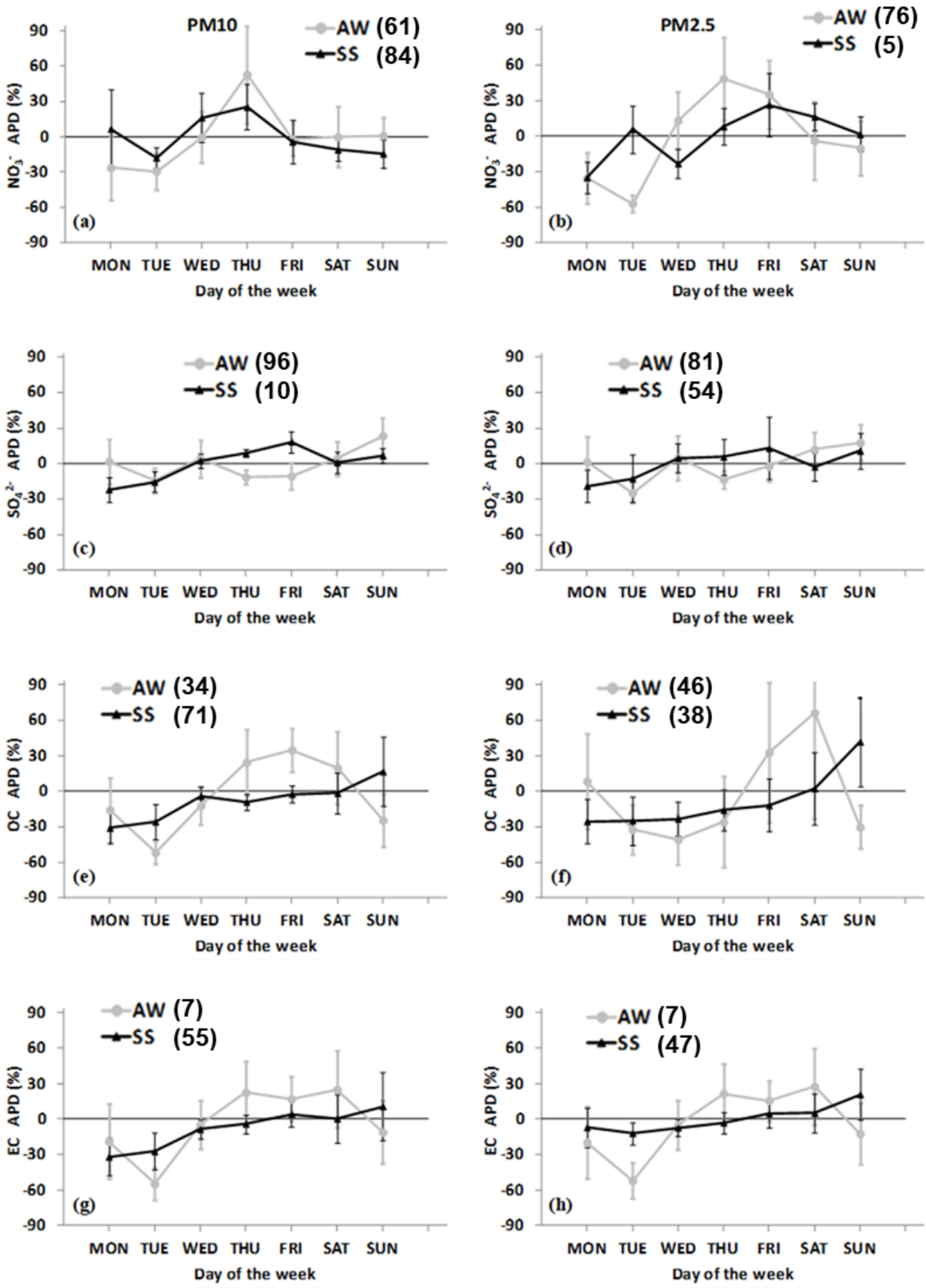

Figure 4. PM10 and PM2.5 Average Percent Departure (APD) of the NO_3^- (a and b, respectively), SO_4^{2-} (c and d, respectively), OC (e and f, respectively), and EC (g and h, respectively) mass concentration as a function of the day of the week and for Autumn-Winter (AW, dots and grey line) and Spring-Summer (SS, triangles and black lines). Error bars represent the standard error of the mean (SEM). The confidence level percentage value of the difference between the Thursday and the Sunday APD for each chemical compound by the Kruskal-Wallis test is reported in brackets.

Figures 3c and 3d highlight that a negative weekly cycle characterizes the NH_4^+-APD values of PM10 and PM2.5 in AW and SS, respectively. The level of confidence (LoC) of the difference between the Sunday and the Thursday-APD value is higher in SS than in AW for PM10 and PM2.5 samples, respectively. Moreover, the PM2.5-LoC value is greater than the PM10-LoC value both in AW and in SS. A marked positive (higher values during weekdays) weekly cycle, supported by the high LoC values, characterizes the Ca^{2+}-APD values of the PM10 and PM2.5 samples both in AW and in SS (Figures 3g and 3h, respectively). A negative weekly cycle (LoC = 79%) characterizes the K^+-APD values of PM10 and PM2.5 samples in SS (black lines, Figures 3e and 3f, respectively). The positive weekly cycle that characterizes the K^+-APD values of the PM10 and PM2.5 samples in AW (grey lines, Figures 3e and 3f, respectively) is not significant.

Figures 4a and 4b highlight that the positive weekly cycle that characterizes the NO_3^--APD values of the PM10 and PM2.5 particles both in AW and in SS is not very significant, unless in SS for the PM10 samples. A significant negative weekly cycle characterizes the SO_4^{2-}-APD values of the PM10 and PM2.5 samples in AW (Figures 4c-d). The OC and EC weekly cycle is not significant (Figures 4e-4h).

In conclusion, Figures 3 and 4 indicate that $NH_4^+$and K^+ likely contribute to the SS negative weekly cycle of the PM10 and PM2.5 mass concentration. The NH_4^+ is a marker of secondary photochemical processes (Calzolai et al., 2015) and K^+ can be associated with combustion emissions. In AW, the positive weekly cycle of Ca^{2+} likely contributes to the positive weekly cycle of PM10 and PM2.5 mass concentrations.

3.3 Source apportionment by Positive Matrix Factorization

For the PM10 dataset, PMF solutions from 4 to 9 factors have been explored and a 6-factor solution was considered to be the most reliable. The optimal solution presented below is obtained by

constraining the base-solution using a sulphate-to-ammonium ratio of 2.7 (i.e. stoichiometrically referred to ammonium sulphate) and pulling up maximally sulphate in the factor associated to the secondary sulphate. The implementation of these constraints has improved a lot the mapping of the factors as retrieved from bootstrap analysis and has given a sum of species not exceeding the PM mass (as required by a physically consistent solution). Finally, scaled residuals result smaller than 3 standard deviations and the PM10 mass is well reconstructed by the model within 10%.

The factor-to-source assignment is tentatively done considering both the percentage of species in the factor (as indication of source tracers when higher than 30%) and the factor chemical profiles (Figure S1, Supplementary Material). Factor 1 is associated to ammonium sulphate due to the high percentage of SO_4^{2-} and NH_4^+. The not negligible percentage of lead in this factor, a result already found by other authors (Taiwo et al., 2014), could be explained with the accumulation of sulphate and nitrate on metal-rich particles (e.g., forming $ZnSO_4$ and $PbSO_4$ particles). Factor 2 is labelled as mixed anthropogenic because of the presence of markers from both traffic (e.g., EC, OC, Cu, Fe, Ba) and biomass burning (e.g., K^+, OC, EC). A more detailed disentanglement of the mixed anthropogenic source (e.g., traffic vs. biomass burning) has not been taken into consideration in order to achieve a better comparability with the results from PM2.5 source apportionment and because not particularly useful for the aim of the present work. Factor 3 is characterized by high EC values for V and Ni, typical tracers of heavy oil combustion (e.g., Mazzei et al., 2006), and their contributions are likely due to pollution from ship emissions (Becagli et al., 2012). In this factor, it is also notable a high percentage of MS^- because of the oxidation of dimethylsulphide emitted by the plankton activity in the sea, thus suggesting the association to a secondary marine source. Previous works have related the concomitant presence of MS^- and sulfur-derived particles, gaseous MS^- condensed onto sea salt and soil-derived particles (Kerminen et al., 1997). Following the results obtained at the same site by Perrone et al. (2013), Factor 4 is labelled as reacted dust, in agreement with the source profiles reported in previous source apportionment studies (e.g., Perrone et al., 2013; Cesari et al., 2014; Bove

et al., 2015; SPECIEUROPE database): indeed, it has signatures from crustal particles mixed with secondary species like the nitrates and sulphates. Factor 5 has Na^+ and Cl^- as typical markers for sea salt particles. Factor 6 shows soil-related elements in high percentages thus suggesting resuspended dust as source (e.g., Al, Ca^{2+}, Sr, Ti, Fe).

The apportionment of the resolved sources to the PM10 mass is as follows (Figure 5a as overall mean percentages): mixed anthropogenic source (40%), sulphate (20%), soil dust (21%), reacted dust (10%), sea salt (8%), and heavy oil combustion/shipping and secondary marine contributions (1%). It is noteworthy that the large majority of the sources here identified are the same as those detected at the study site by Perrone et al. (2013).

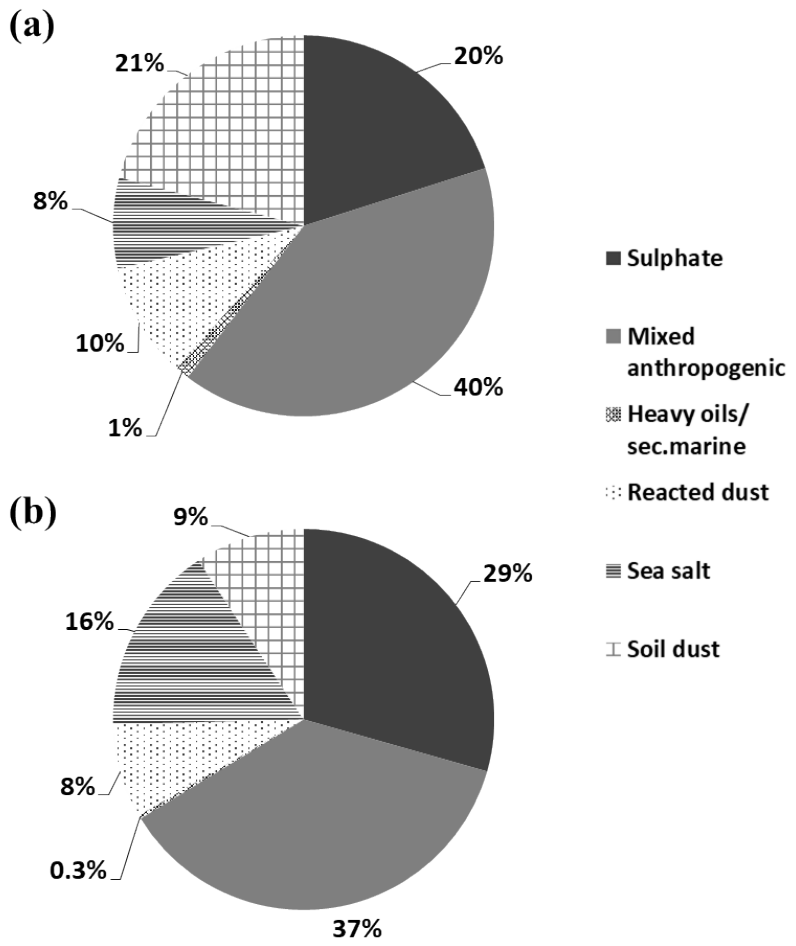

437

438 **Figure 5.** Apportionment of the resolved sources in (a) PM10 and (b) PM2.5.

439

440 The PM2.5 dataset has been similarly analyzed and a 6-factor solution has been chosen (Figure S2,
441 Supplementary Material). The base-case solution is constrained exactly as done for the PM10 and the
442 final solution has been improved in both the factor mapping and the mass reconstruction. The solution
443 presented in the following shows scaled residuals for chemical components smaller than or equal to
444 3 standard deviations in almost all cases (except 9 cases out of 2160 that were smaller than 3.5). The
445 agreement between the reconstructed and modelled PM2.5 values is satisfactory, i.e. within 10%. The
446 factor-to-source assignment has been performed according to the same criteria described above for
447 the PM10 solution and using the same tracers. Thus, by taking into account the chemical profiles
448 (Figure S2, Supplementary Material) and the component percentages in each factor, the 6 factors are

449 related to the mixed anthropogenic source (37%), sulphate (29%), sea salt (16%), soil dust (9%),
450 reacted dust (8%), and heavy oil combustion/shipping and secondary marine contributions (0.3%), as
451 reported in Figure 5b. The high relative contribution of sea salt can be ascribed to secondary
452 components (i.e. OC, sulphate, nitrate, and ammonium), which give non negligible contributions to
453 the chemical profile compared to PM10 results.

454 The percentage contribution of the 23 aerosol chemical components inserted in the PMF analysis to
455 each identified pollution source is shown in Figures S3a and S3b of the Supplementary Material for
456 the PM10 and PM2.5 particles, respectively.

457

458 *3.3.1 Seasonal dependence of the PM10 and PM2.5 aerosol sources*

459 Figure 6 shows the mean mass percentage of the six sources identified by the PMF technique for AW
460 (dark grey bars) and SS (light grey bars) and for (a) PM10 and (b) PM2.5, highlighting that the source
461 seasonal dependence is rather similar for PM10 and PM2.5 particles. The mixed anthropogenic is the
462 dominant pollution source in AW contributing with 57 and 54% to the PM10 and PM2.5 mass,
463 respectively. It is characterized by high contributions due to the OC, EC, NO_3^-, and K^+, which are
464 dominant chemical components of the PM10 and PM2.5 samples in AW, in addition to the SO_4^{2-}
465 (Table 1). The contribution of the mixed anthropogenic source decreases more than 50% in SS
466 because of the decrease of the OC, EC, NO_3^-, and K^+ mass percentages from AW to SS, both in the
467 PM10 and in the PM2.5 samples. The decrease of the residential heating contribution from AW to SS
468 likely contribute to this result. Sulphate, soil dust, and mixed anthropogenic sources contribute almost
469 equally to the PM10 mass in SS (i.e. 27, 25, and 26%, respectively, see Figure 6). The sulphate source
470 is characterized by the high SO_4^{2-} and NH_4^+ contributions, which generally increase by about 50%
471 from AW to SS, both in the PM10 and in the PM2.5 samples, because of the enhanced photochemical
472 processes and the low air mass replacement occurring in SS over the Mediterranean (Querol et al.,

2009). The sulphate is by far the dominant pollution source of the PM2.5 particles in SS, contributing with 42% to the PM2.5 mass (Figure 6b).

The low frequency of rainy days occurring in SS over the Mediterranean Basin is responsible for the enhanced natural and anthropogenic dust resuspension, the limited removal of atmospheric particles by wet deposition and, hence, the air mass aging (Perrone et al., 2015). Consequently, the PM10 soil dust source increase from 16% in AW to 25% in SS. In AW and SS, the soil dust source almost equally contribute in the PM2.5 samples (about 10%).

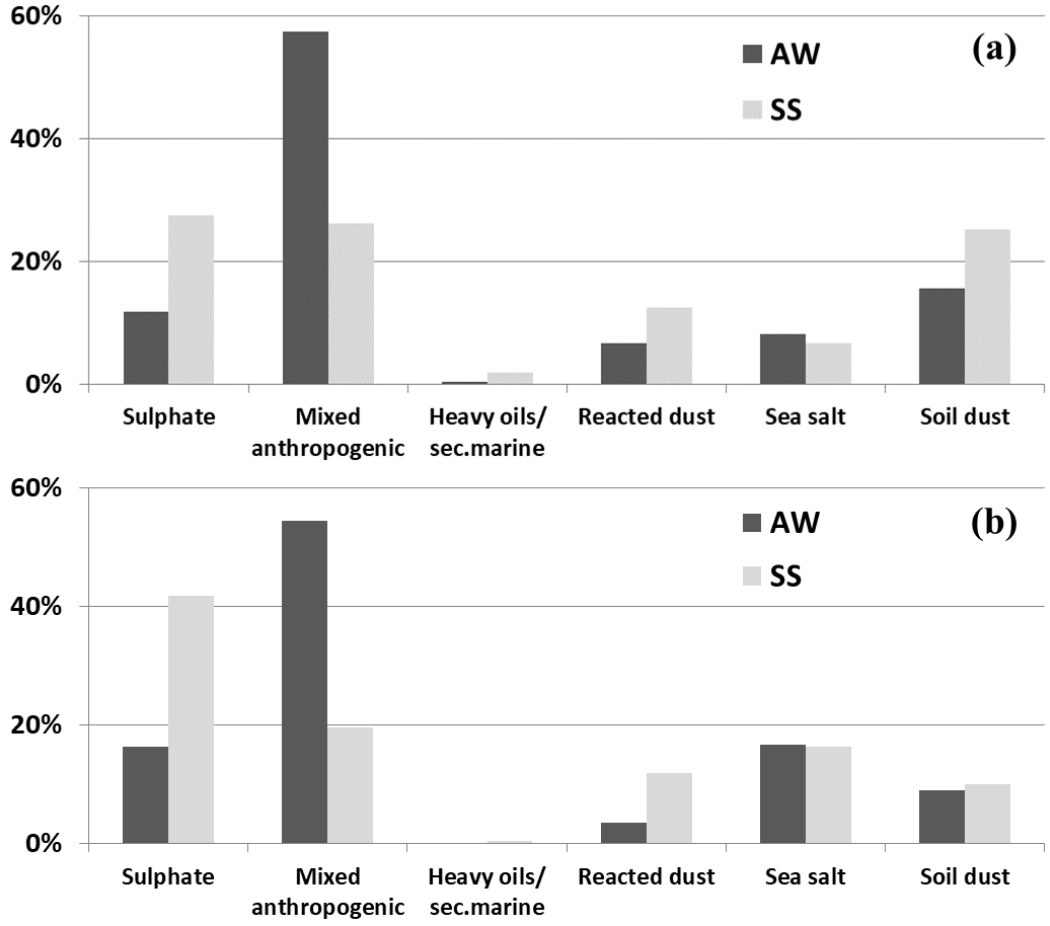

Figure 6. Mean mass percentage of the six sources identified by the PMF technique for Autumn-Winter (AW, dark grey bars) and Spring-Summer (SS, light grey bars) and for (a) PM10 and (b) PM2.5 particles.

3.3.2 Weekly cycle of the PM10 and PM2.5 pollution sources in AW and SS

The pollution source contributions on Thursday (mid-week day) and Sunday are compared to detect the weekly cycle of the identified pollution sources and obtain a better understanding of the PM10 and PM2.5 weekly cycle both in AW and in SS. The highest weekday APD value is reached on Thursday in AW for the PM10 and PM2.5 particles. Conversely, it is reached on Sunday in SS. Note that the comparison of data referring to two different days of the week allow a data treatment based on equal numbers of PM samples.

Figures 7 and 8 show the mean mass percentage of the PM10 and PM2.5 sources, respectively, on Thursday (dark grey bars) and Sunday (light grey bars) and for (a) AW and (b) SS. Due to the limited number of available data for Thursdays and Sundays, it has to be taken into account that variability

associated to sources contribution is non negligible and the weekly cycle here presented is to be considered as a first guess. As an example, the sea salt contribution in PM10 during SS shows a marked difference that has to be ascribed to a huge episode of air mass transport from the sea (see section 3.6).

A quick look at Figures 7 and 8 highlights that the weekly cycle of the identified pollution sources varies with the PM fraction and that the sources exhibit different weekly variability for different seasons, in reasonable accordance with the results by Georgoulias and Kourtidis (2011;2012).

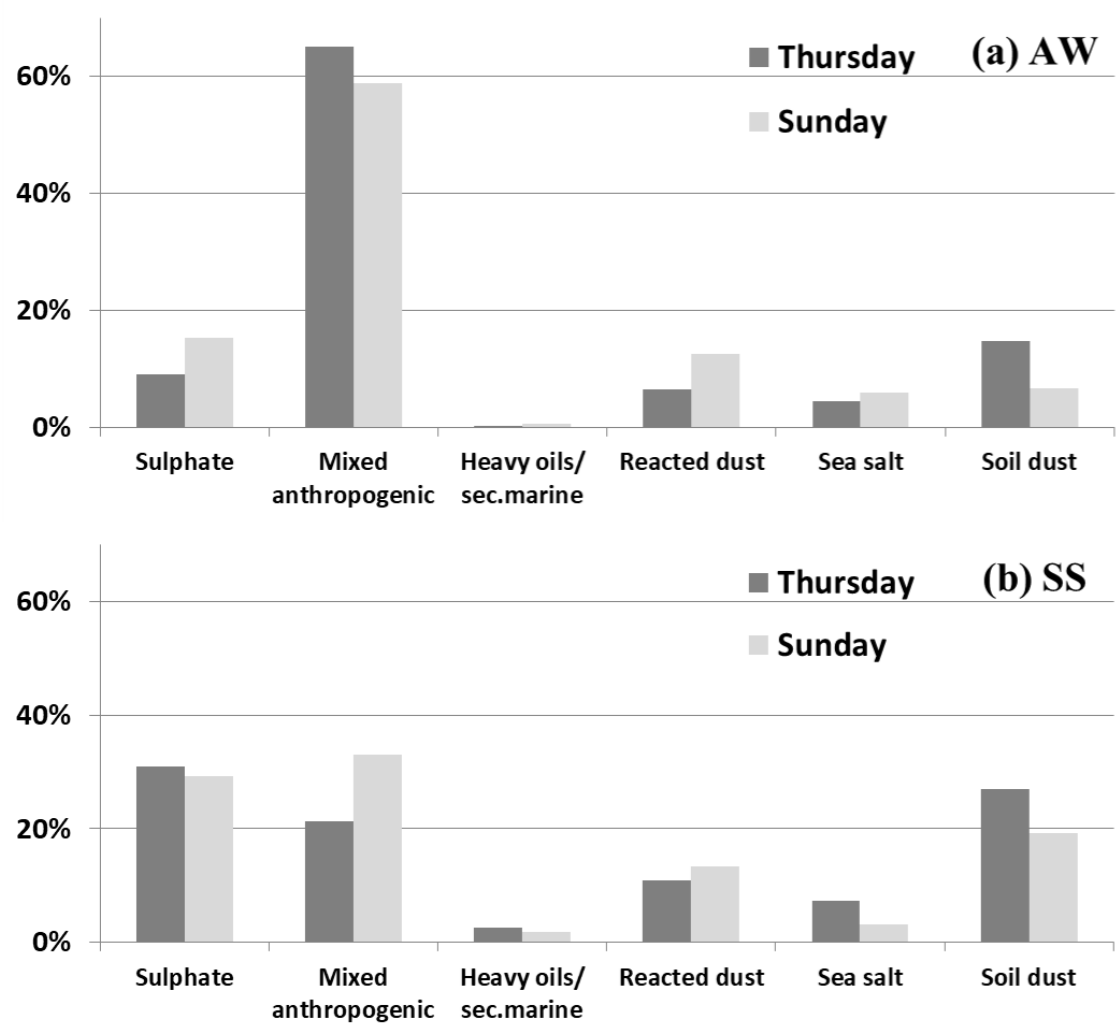

505

506 **Figure 7.** Mean mass percentage of the PM10 sources on Thursday (dark grey bars) and Sunday (light grey bars) and for
507 (a) Autumn-Winter (AW) and (b) Spring-Summer (SS).

508

509 Figure 7 shows that in AW the sulphate and reacted dust contribution to the PM10 mass is a bit larger
510 on Sunday than on Thursday. Conversely, the contribution of both the mixed anthropogenic and the
511 soil dust source is greater on Thursday than on Sunday, thus contributing to the PM10 positive weekly
512 cycle found in AW. As shown in Figure 3g, it is noteworthy that Ca^{2+} is the main species contributing
513 to both sources, which is characterized by a significant positive weekly cycle in AW.

514 In SS, the contribution of the mixed anthropogenic source is greater on Sunday than on Thursday and
515 it is likely responsible for the PM10 negative weekly cycle found in SS. As represented in Figure 3e,

516 K^+ is the species contributing to the mixed anthropogenic source that is characterized by a significant
517 negative weekly cycle in SS.

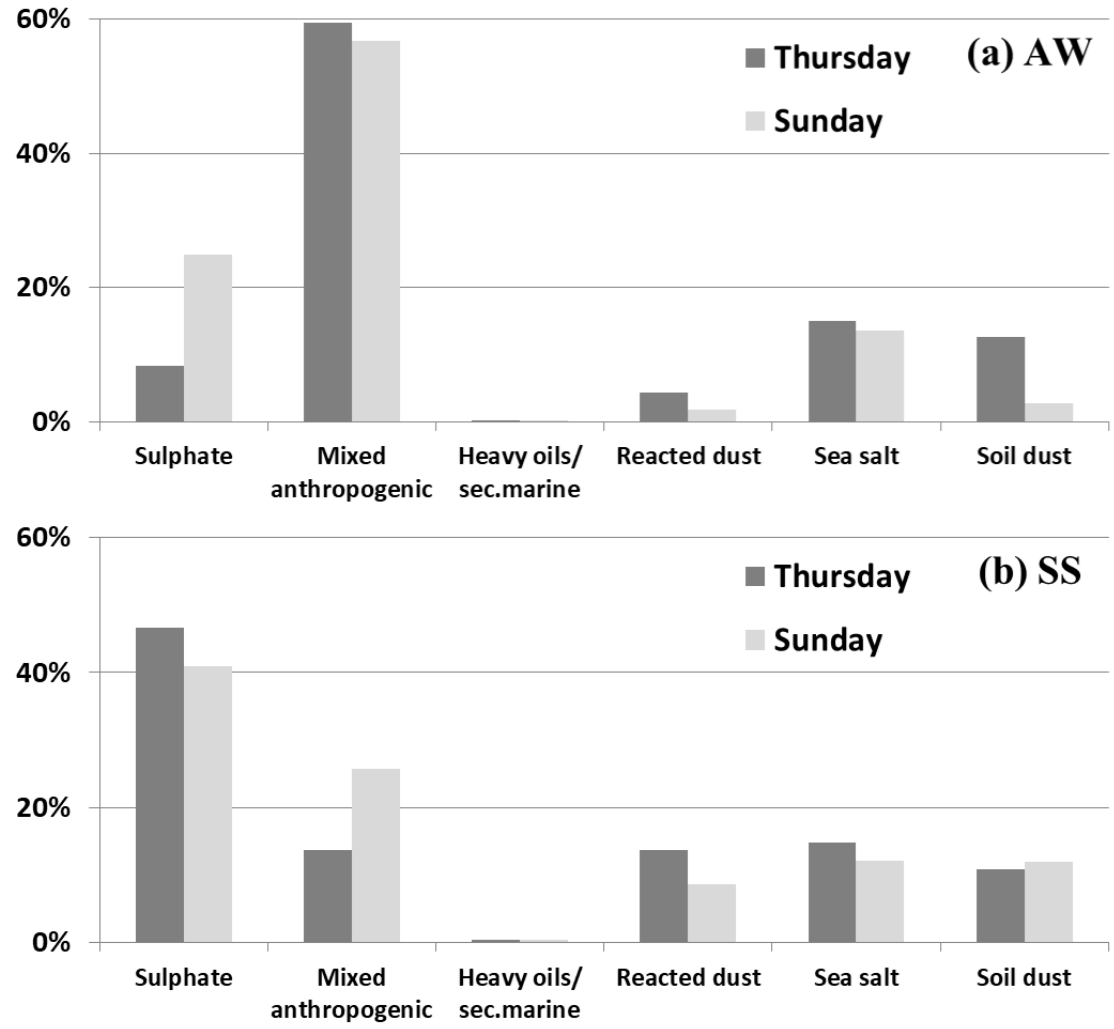

518

519 **Figure 8.** Mean mass percentage of the PM2.5 sources on Thursday (dark grey bars) and Sunday (light grey bars) and for
520 (a) Autumn-Winter (AW) and (b) Spring-Summer (SS).

521

522 The mixed anthropogenic source likely also contribute to the PM2.5 negative weekly cycle observed
523 in SS (Figure 8). The PM2.5-K^+ is also characterized by a significant negative weekly cycle in SS
524 (Figure 3f).

525 The soil dust, reacted dust, and mixed anthropogenic sources likely contribute to the positive PM2.5
526 weekly cycle observed in AW. Note that Ca^{2+} (Figure 3h) and NO_3^- (Figure 4b) are dominant

components of the soil dust, reacted dust, and mixed anthropogenic sources, respectively, and are both characterized by a positive weekly cycle in AW.

The sulphate source contribution is higher on Sunday than on Thursday in AW (Figures 7a and 8a). It deserves particular attention being on average one of the main sources contributing to the PM. NH_4^+ and SO_4^{2-} are the dominant species contributing to the sulphate source: both chemical components are characterized by a significant negative weekly cycle in AW (Figures 3c-d and 4c-d, respectively) and are dominant in the fine fraction (Table 1). Consequently, the main features of the sulphate source are similar for PM10 and PM2.5 particles (Figures 6-8). SO_4^{2-} and NH_4^+ are markers of secondary photochemical processes and, because of this, their contribution is likely greater on Sunday than on the working days. Wagstrom and Pandis (2009) have investigated the age distribution of primary and secondary aerosol species using a chemical transport model. They defined the aerosol age as the time that elapsed since a particle (or its precursor) entered the atmosphere and found over a polluted continental region of the United States that primary aerosol species had average ages of approximately 24 h, while the average ages for secondary species were 48-72 h near the surface. They also found that the average age of all aerosol components increase vertically in the atmosphere. The westerly transport of pollution at the study site during the weekend could also have contributed to the negative weekly cycle of the SO_4^{2-} and NH_4^+ found in AW, based on Georgoulias and Kourtidis (2011) and Perrone et al. (2015). In SS, the enhanced photochemical processes and the low air mass renovation occurring all over the Mediterranean Basin are responsible for the strong increase (more than 50%) of the sulphate source contribution (e.g., Querol et al., 2009). Moreover, Miyakawa et al. (2007) observed that the average formation efficiency of SO_4^{2-} is six times greater in summer than in winter and that the SO_x lifetime is about two times longer in summer than in winter.

3.4 Detection of the weekly cycle in the NO_2 mass concentrations

551 Nitrogen oxides -NO and NO_2- are important precursors responsible for the secondary aerosol
552 production through gas-to-particle conversion processes (Seinfeld and Pandis, 1998; Jacobson and
553 Kaufman, 2006). NO_2 is emitted in small quantities from combustion processes along with NO and it
554 is largely formed in the atmosphere by the oxidation of NO (Seinfeld and Pandis, 1998). Most of NO_2
555 in cities comes from motor vehicle exhaust. Other sources of NO_2 are petrol and metal refining,
556 electricity generation from coal-fired power stations, domestic heating, manufacturing industries, and
557 food processing. Nitrogen oxides, whose occurrence is closely related to human activities, influence
558 chemical and biological processes both locally and globally (e.g., Hayn et al., 2009 and references
559 therein). Hayn et al. (2009) have analyzed spatio-temporal patterns of the global NO_2 distribution
560 from satellite observations (1996-2001). In particular, they have found that clear weekly cycles
561 appeared in urban areas indicating anthropogenic sources and that the significance of the weekly cycle
562 changed on smaller spatial scales than, for example, the annual cycle.
563 The daily average of NO_2 mass concentration for the sampling days of this study is obtained from the
564 Regional Air Quality monitoring station in Arnesano (http://www.arpa.puglia.it/pentaho/ViewAction
565 ?solution=ARPAPUGLIA&path=metacatalogo&action=meta-aria.xaction), which is ~500 m away
566 from the study site. The mean of NO_2 mass concentration is equal to 32 and 22 μg m^{-3} in AW and SS,
567 respectively. Figure 9 shows the average percent departure of the NO_2 concentrations for AW (grey
568 lines) and SS (black lines). Error bars represent the standard error of the mean (SEM). A positive
569 weekly cycle characterizes the NO_2-APD values in AW. The Friday-APD value is 31% greater than
570 the Sunday-APD value and the difference is significant at the 87% confidence level (KW-test, Table
571 2). A negative weekly cycle characterizes the NO_2-APD values in SS. The Sunday-APD value is 39%
572 greater than the Wednesday-APD value and the difference is significant at the 96% confidence level
573 (KW-test, Table 2). The comparison of Figure 9 with Figures 2a and 2b shows that the NO_2-APD
574 weekly evolution is rather similar to that of the PM10- and mainly the PM2.5-APD values both in
575 AW and in SS. This result likely indicates that NO_2 is largely due to the aerosol sources responsible
576 for the PM weekly cycle both in AW and in SS. In fact, NO_2 is mostly emitted from motor vehicle

577 exhaust, electricity generation from coal-fired power stations, domestic heating, and manufacturing
578 industries (Stjern, 2011) and, in the urban pollution plumes, aerosols generate a remarkable increase
579 of the surface NO_2 via reducing its photolytic loss and diffusion in the boundary layer, based on Li et
580 al. (2017) and references therein.
581 Hayn et al. (2009) found that a positive weekly cycle characterized the NO_2 tropospheric vertical
582 column density (TVCD) over Europe, without differentiating the data with seasons. In particular, a
583 closer look at the day of the minimum NO_2-TVCD in the plume of large anthropogenic sources with
584 a strong weekly cycle revealed a west-east translation of the weekly NO_2 minimum. In particular, the
585 original Sunday minimum in western Europe (5°E-15°E) moved eastwards with the dominating west
586 wind and it was observed on Monday in east Poland (20°-23°E). The findings by Hayn et al. (2009)
587 are in reasonable agreement with the ones of this study found in AW, when the NO_2 mass
588 concentration reached the highest mean seasonal value at the study site.
589

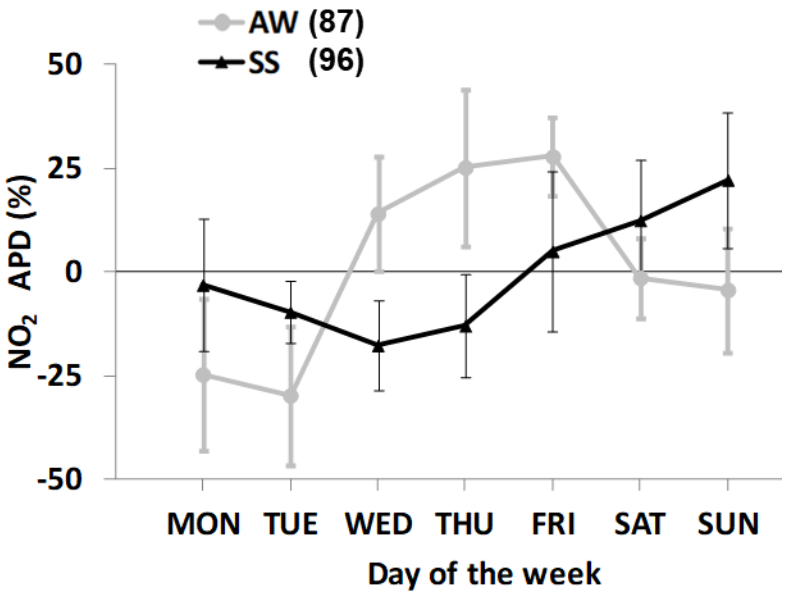

590

591 **Figure 9.** Average Percent Departure (APD) of the NO_2 mass concentration as a function of the day of the week and for
592 Autumn-Winter (AW, dots and grey line) and Spring-Summer (SS, triangles and black lines). Error bars represent the
593 standard error of the mean (SEM). The confidence level percentage of the difference between the Friday and the Sunday
594 APD for AW and between the Wednesday and the Sunday APD for SS by the Kruskal-Wallis test is reported in brackets.

595

596 *3.5 Weekly cycle of the near-surface temperature and wind speed*

597 Temperature and wind speed measurements, co-located in space and time with the PM measurements,
598 are analyzed to identify the weekly cycle in meteorological parameters and investigate their
599 relationship with the PM weekly cycle. Aerosol particles are known to affect temperature and wind
600 speed at the surface, even if the aerosol impact on meteorological parameters is still controversial
601 (e.g., Gong et al., 2007; Sanchez-Lorenzo et al., 2012). T and WS hourly means from a local
602 meteorological station at about 10 m from the ground level are averaged to obtain a daily mean value.
603 The T and WS means are equal to 12.7 °C and 1.6 m s^{-1}, respectively, in AW and 20.4 °C and 2.7 m
604 s^{-1}, respectively, in SS. The T- and WS-APD values are calculated in accordance with Eq. 1. Figures
605 10a and 10b show the T- and WS-APD weekly evolution with corresponding SEMs, respectively, for
606 AW (grey lines) and SS (black lines). A quick look at Figure 10 reveals that the day-by-day changes

607 of T and WS are greater in AW than in SS, as the PM-APD values also show (Figure 2), likely
608 suggesting the existence of a relationship between the PM and the T and WS changes.

609

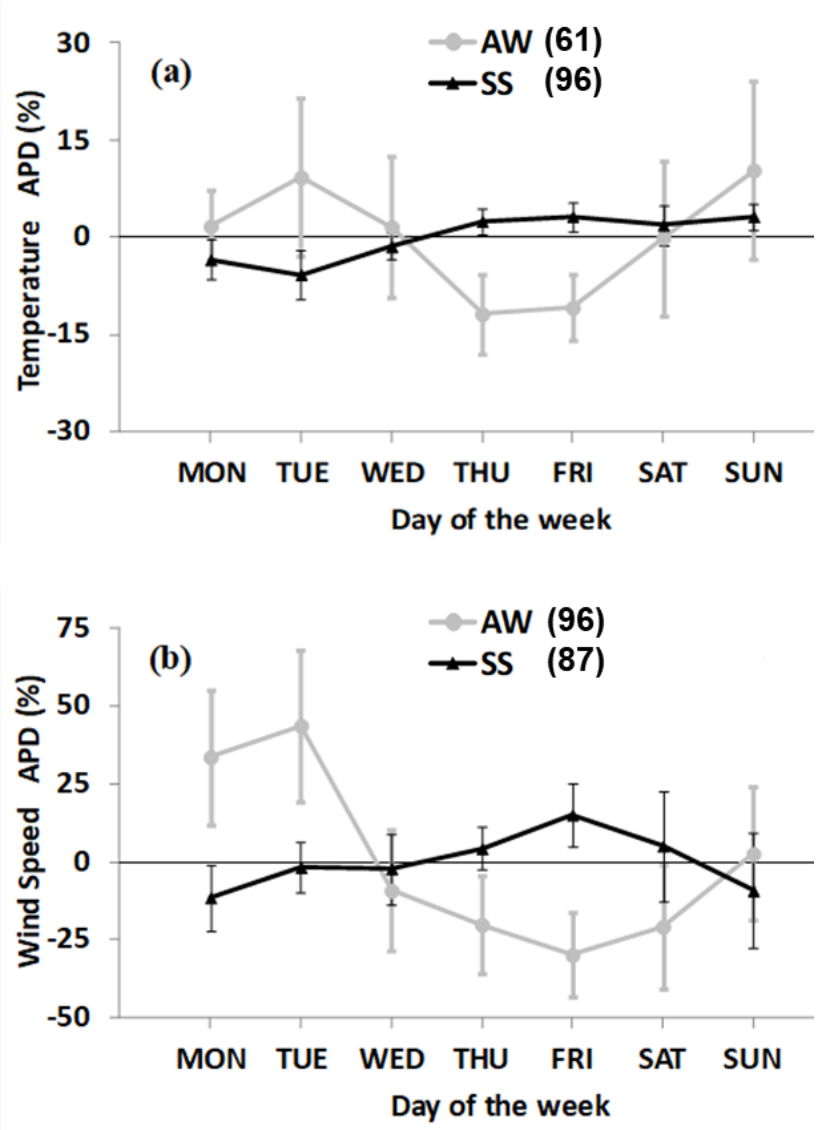

610

611 **Figure 10.** Average Percent Departure (APD) of the (a) air temperature (T) and (b) wind speed (WS) as a function of the
612 day of the week and for Autumn-Winter (AW, dots and grey line) and Spring-Summer (SS, triangles and black lines).
613 Error bars represent the standard error of the mean (SEM). The confidence level percentage of the difference between the
614 Thursday and the Sunday T-APD for AW and between the Tuesday and the Sunday T-APD for SS by the Kruskal-Wallis
615 test is reported in brackets in (a). The confidence level percentage of the difference between the Tuesday and the Friday
616 WS-APD for AW and between the Monday and the Friday WS-APD for SS by the Kruskal-Wallis test is reported in
617 brackets in (b).

618

619 A clear negative weekly cycle characterizes the T-APD values in AW. The Sunday T-APD value is
620 more than 20% greater than the Thursday value but the difference is not significant (Table 2). The

621 decrease of the T daily mean values on the mid-week days likely gives evidence of the PM cooling
622 effect at the surface (e.g., Jacobson 1998; Jacobson and Kaufman, 2006) because of the increase of
623 the PM mass concentrations up to Thursday (Figure 2). During the day, absorbing and scattering
624 aerosol particles may contribute to the solar radiation reduction to the ground. Moreover, Jacobson
625 (1998) has shown that, during the day and night, all boundary-layer particles radiatively warm the
626 surface and that aerosols affect temperatures primarily through ground-atmosphere turbulent heat
627 transfer. The link between solar irradiance, meteorological parameters, and aerosol properties at the
628 surface has been investigated at the study site during the March 20, 2015 solar eclipse (Romano et
629 al., 2017) and the December 3, 2015 Etna volcano's eruption (Romano et al., 2018), whose main
630 results are in accordance with the findings of Jacobson (1998).

631 The working-day anthropogenic activities contribute to the PM positive weekly cycle in AW, as
632 observed worldwide (e.g., Barmpadimos et al., 2011). Moreover, the mixed anthropogenic is the
633 dominant source in AW and the combustion particles, which have a large impact on solar radiation
634 by scattering and absorption processes, are the main components of this source. Note that a significant
635 negative correlation characterizes the relationship between the PM mass concentrations and
636 corresponding T values in AW. The Pearson correlation coefficients are equal to -0.37 ($p < 0.02$) and
637 -0.42 ($p < 0.01$) for the 41 PM10 and PM2.5 samples, respectively.

638 A weak positive weekly cycle characterizes the T-APD values in SS (Figure 10a, black line). The T-
639 APD values vary from -6% in the first days of the week to about 3% in the second part of the week.
640 The negative PM weekly cycle observed in SS and the changes of the PM optical and chemical
641 properties and/or aerosol source properties from AW to SS (Figure 6) likely contribute to the T weekly
642 cycle in SS. The sulphate is the dominant source in SS and it is mainly contributed by fine non-
643 absorbing particles (Seinfeld and Pandis, 1998). One must also be aware that the mean near-surface
644 T is about 10 °C higher in SS than in AW (Perrone et al., 2013, 2015) and, because of this, the sign
645 of the PM impact on T is likely less relevant in SS. A significant positive correlation is found in SS

between both the PM10- and the PM2.5-APD values and the corresponding T-APD values. The Pearson correlation coefficients are 0.87 ($p < 0.02$) and 0.82 ($p < 0.05$) for PM10 and PM2.5, respectively.

Figure 10b shows that the WS is characterized by a notable negative and positive weekly cycle in AW and SS, respectively. More specifically, in AW, the WS-APD reaches the highest value (44%) on Tuesday and the smallest (-30%) on Friday and the level of confidence of the difference is 96% (KW-test, Table 2). Note that the highest PM-APD value is reached on Thursday in AW (Figure 2). In SS, the WS-APD values increase from Monday (-11%) to Friday (15%) and then decrease up to Sunday (-9%), when the PM-APD reaches the highest value. The level of confidence of the difference between the Friday and the Monday WS-APD values is 87% (KW-test, Table 2). In AW, a significant negative correlation is found between both the PM10 and the PM2.5 mass concentrations and the corresponding WS values. The Pearson correlation coefficients are -0.65 ($p < 0.001$) and -0.66 ($p < 0.001$) for the 41 PM10 and PM2.5 samples, respectively. Conversely, any significant correlation of WS with the PM is found in SS. The changes of the particle optical and microphysical properties from AW to SS likely contribute to this last result.

As mentioned, Romano et al. (2017) have recently investigated the effects of the partial solar eclipse of March 20, 2015 on the near surface meteorological variables at three coastal sites of southern Italy, including the monitoring site of this study. They have found that the solar eclipse was responsible at the study site for a T decrease within 0.5–0.8 K and a WS decrease within 0.5–1.0 m s^{-1} because of its cooling effect. Similar results were found at the other two sites. We believe that the cooling effect at the surface due to an eclipse is to some extent similar to that due to an aerosol cloud. Consequently, the results by Romano et al. (2017) could further support those of this study.

Scientific papers regarding the aerosol particle effect on surface wind are scarce, based on Barò et al. (2015). They have performed numerical simulations for Europe during the Russian fires from July 25 to August 15, 2010. The results showed that the presence of aerosol reduced the wind speed module

671 over Russia. More specifically, they have observed that the aerosol radiative effects decreased the
672 shortwave radiation at the surface, leading to a reduction of the T monitored at 2 m above the ground
673 level. Because of that, convective processes and turbulence decreased, developing a more stable
674 planetary boundary layer with lower heights and reducing WS. However, they have found that the T
675 decrease over Central Europe was responsible for a surface pressure decrease and a WS increase.
676 Jacobson and Kaufman (2006) have investigated the WS reduction due to aerosol particles by
677 numerical models. They have observed that aerosol particles and aerosol-enhanced clouds decreased
678 near-surface air temperatures, increased stability, and reduced turbulent kinetic energy (TKE). Then,
679 the reduced TKE helped to reduce WS over land near the coast, increasing convergence of offshore
680 WS as well. Jacobson and Kaufman (2006) have performed simulations over a regional costal area in
681 California (USA).

682 Gong et al. (2007) have reported different results from observations of individual stations in seriously
683 polluted east China. They have found that stronger winds on Thursday and Friday followed the PM10
684 maximum of Wednesday. They have hypothesized that during the early part of the week the
685 gradually-accumulated anthropogenic aerosol induced radiative heating, likely destabilizing the
686 middle to lower troposphere and generating anomalously vertical air motion and thus resulting in
687 stronger winds. The resulting circulation could promote ventilation to reduce aerosol concentrations
688 in the boundary layer during the latter part of the week. The above comments show that the
689 uncertainties regarding the underlying aerosol-meteorology feedback still exist likely because of the
690 significant role played by the geographical location of the monitoring site and the particle chemical
691 properties (Romano et al., 2017). Consequently, studies as the one reported in this paper, which likely
692 display the PM signal on meteorological data, are essential to improve the knowledge of the
693 underlying aerosol-meteorology feedback.

694

695 *3.6 Results from a case study: April 6-12, 2015*

696 The main results on PM10 and PM2.5 mass concentrations and T and WS daily means monitored at
697 the study site during the April 6-12, 2015 week are discussed in this sub-section to highlight the
698 impact of the long-range transport on PM mass concentrations by a case study and display the T and
699 WS daily change. Figure 1 shows the pathways of the four-day analytical back trajectories that
700 reached the study site at 500 m above sea level (asl) at 12:00 UTC of each day of the week. The back
701 trajectories calculated at 00:00, 06:00, 12:00, and 18:00 UTC of each day of the week are provided
702 in the Supplementary Material (Figure S4). Analytical back trajectories are calculated from the
703 Hybrid Single Particle Lagrangian Integrated Trajectory (HYSPLIT) Model (Draxler and Rolph,
704 2003). Figure 1 shows that air masses from the west reached the study site on Monday, while air
705 flows that crossed northeastern European regions reached the study site from Tuesday to Sunday. The
706 PM10 and PM2.5 mass concentrations increase with the day of the week from 14 and 11 μg m^{-3},
707 respectively, on Monday to 45 and 34 μg m^{-3}, respectively, on Sunday. Figure 11a shows that the
708 PM10 (grey triangles) and PM2.5 (black dots) APD values are representative of a negative weekly
709 cycle (Figure 2, black dots). These last results are in accordance with those from Perrone et al. (2013,
710 2015), which show that the low PM mass concentrations are generally associated with the west
711 airflows. Conversely, the largest PM mass concentrations are generally associated with northeastern
712 air flows, which are also responsible for the advection of fine mode particles due to sulphate and
713 traffic sources, as Lelieveld et al. (2002) and Querol et al. (2009) also suggest for the Mediterranean
714 Basin. Figure 12 shows the daily mean mass concentrations of some dominant chemical components
715 as (a) K^+, (b) EC, (c) OC, and (d) SO_4^{2-} during the April 6-12, 2015 week, for the PM10 (grey dots)
716 and PM2.5 (black triangles) particles. Figure 12 highlights both that the tested species are mainly in
717 the fine fraction and that the mean mass concentrations of K^+, EC, and OC (associated with a traffic
718 source) and SO_4^{2-} generally increase with the day of the week supporting the above reported
719 comments. Figure 13 shows the mean mass percentage of the identified aerosol sources on Thursday
720 April 9 (dark grey bars) and Sunday April 12 (light grey bars) for (a) PM10 and (b) PM2.5 particles.

721 The mixed anthropogenic and sulphate sources likely significantly contribute to PM10 and PM2.5 on
722 Sunday.

723 Figure 11b shows the T- (grey triangles) and WS-APD (black dots) values during the April 6-12,
724 2015 week. The weekly mean of T and WS is 11 °C and 4 m s^{-1}, respectively. The T-APD values on
725 average increase with the PM-APD values since Tuesday. Conversely, the WS-APD decreases fast
726 with the day of the week since Wednesday. Likely, Figure 11b also gives evidence of a possible PM
727 impact on the local meteorology.

728

729

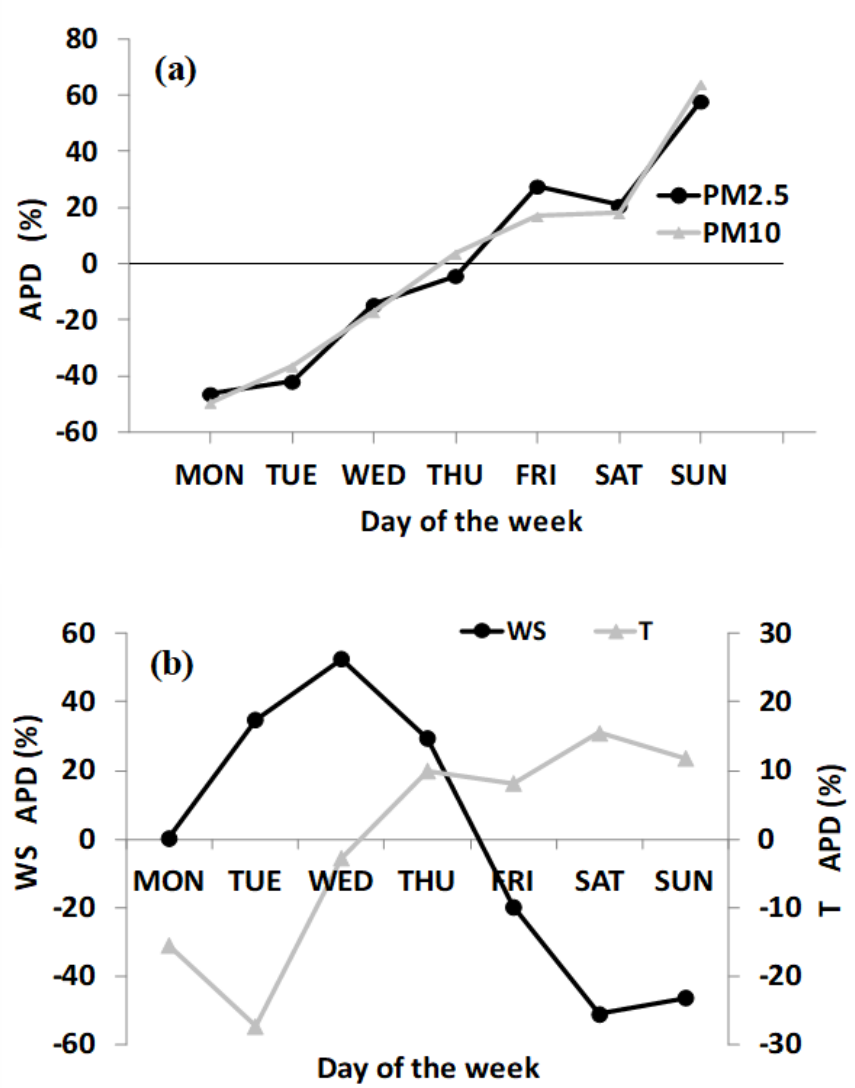

730

731 **Figure 11.** Average Percent Departure (APD) of the (a) PM10 (grey triangles) and PM2.5 (black dots) mass
732 concentrations and the (b) air temperature (T, grey triangles) and wind speed (WS, black dots) as a function of the day of
733 the week April 6-12, 2015.

734

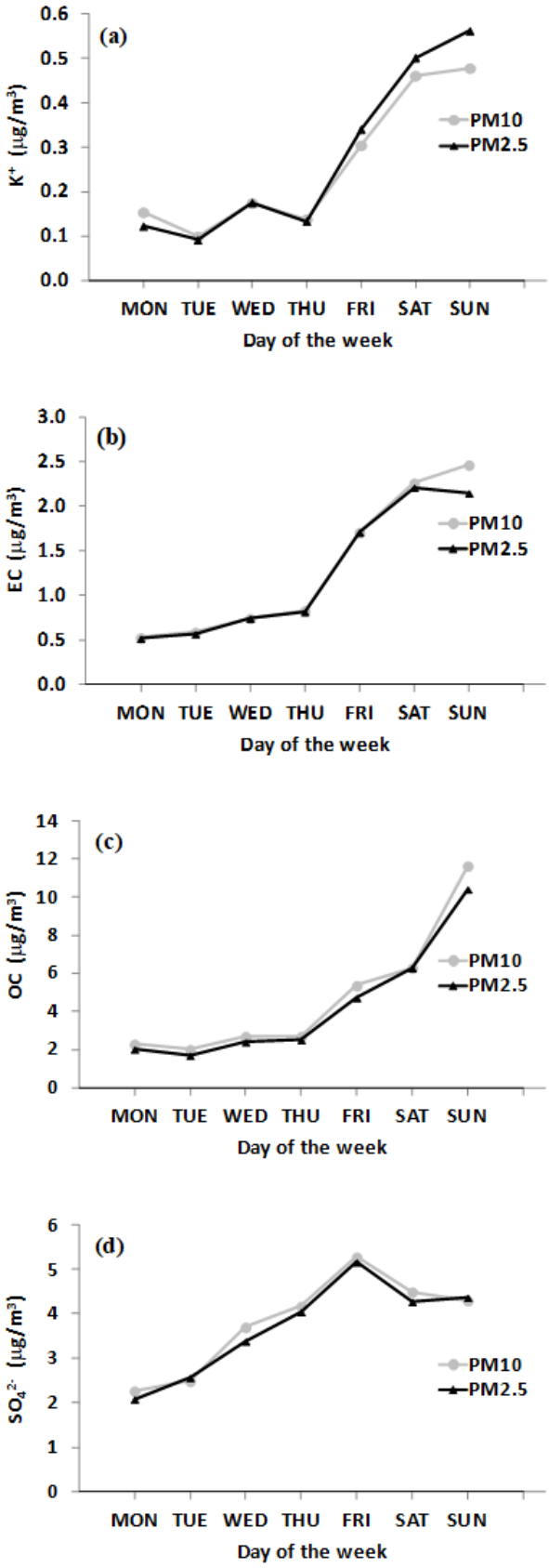

735

736 **Figure 12.** Daily mean mass concentrations of (a) K^+, (b) EC, (c) OC, and (d) SO_4^{2-} during the week April 6-12, 2015,
737 and for PM10 (grey dots) and PM2.5 (black triangles) particles.

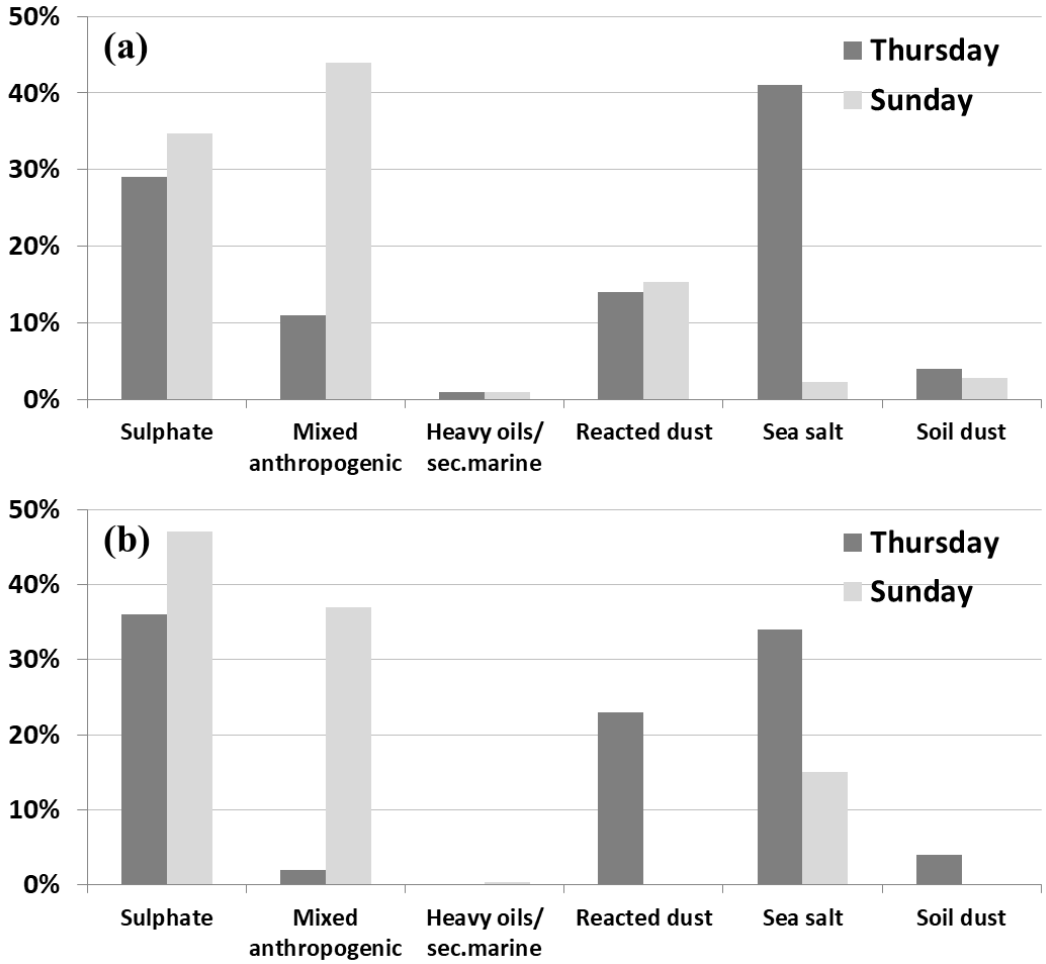

738

739 **Figure 13.** Mean mass percentage of the (a) PM10 and (b) PM2.5 sources on Thursday April 9, 2015 (dark grey bars)
740 and on Sunday April 12, 2015 (light grey bars).

741

742 ## 4. Summary and conclusion

743 Chemically speciated PM10 and PM2.5 samples collected over one year (October 2014 - October
744 2015) are analyzed in this study to present a methodology that allows identifying the PM weekly
745 cycle in SS and AW and single out their possible role on the near surface temperature and wind speed.
746 The PMF technique is applied to chemically speciated PM samples to retrieve major aerosol sources
747 affecting the study area and likely assess their impact on the PM weekly cycle both in AW and in SS.
748 A 6-factor solution is the most reliable for both the PM10 and PM2.5 particles because of the large

749 contribution of fine particles at the study site. On average, 71 and 76% of the PM10 mass
750 concentration is accounted for by the PM2.5 particles in AW and SS, respectively.

751 • A positive (higher values during midweek) and negative (higher values during weekend) weekly
752 cycle characterizes the PM10 and PM2.5 mass concentrations in AW and SS, respectively. The
753 westerly long-range transport of pollution is likely contributing to the PM negative weekly cycle
754 observed in SS. Results from a case study support the above comment.

755 • The mixed anthropogenic source likely contribute to the PM10 and PM2.5 negative weekly cycle,
756 in SS.

757 • In AW, the mixed anthropogenic and soil dust sources likely contribute to the positive weekly cycle
758 of the PM10 particles, while the mixed anthropogenic, soil dust, and reacted dust sources likely
759 contribute to the PM2.5 positive weekly cycle.

760 • The negative and positive weekly cycles, which characterized the NO_2 mass concentrations in SS
761 and AW, respectively, suggest that NO_2 is largely due to the aerosol sources responsible for the PM
762 weekly cycle.

763 • The analysis of the near surface T and WS seems to display the PM signal on meteorological data:

764 - a clear negative weekly cycle characterizes the near-surface T- and WS-APD values in AW
765 likely giving evidence of the PM cooling effect on weekdays, which decreases the near surface
766 T, increases the stability, reduces the turbulent kinetic energy, and decreases the WS.

767 - a positive weekly cycle characterizes the near-surface T- and WS-APD values in SS likely
768 because of the negative PM weekly cycle and the changes of the particle optical and microphysical
769 properties from AW to SS.

770 In conclusion, the work shows the existence of a PM weekly cycle dependent on seasons at a coastal
771 site of the Central Mediterranean. The westerly long-range transport of pollution has likely

772 contributed to the observed PM weekly cycle, in accordance with previous studies. The notable and
773 consistent seasonal variability of meteorological parameters and PM mass concentrations and the
774 good correlations between them could be a sign of the aerosol impact on the local meteorology. The
775 changes of the PM chemical, optical, and microphysical properties from AW to SS, in addition to the
776 local and synoptic meteorology, have likely contributed to the observed results. We believe that
777 studies as the one of this paper are essential either to improve the knowledge of the underlying
778 aerosol-meteorology feedback and to further contributing to the characterization of the aerosol main
779 features over the Mediterranean Basin, which is a hot spot in climate change studies. Paper's results
780 come from a single year of measurements and this may represents a questionable aspect, since it could
781 have an impact not only on the statistical significance, but also on the "representativeness" of the
782 results: weekly cycle variability may change with the passing of the years. However, we believe that
783 the results from a single year of measurements could have the advantage to better single out the sign
784 of the aerosol impact on the local meteorology. The PM-to-meteorology link is non-linear and
785 contains potentially cancelling mechanisms, challenging the discovery of an aerosol signal in
786 meteorological data when, for example, results related to many years add up. Work is in progress in
787 this direction.

788

789 **Acknowledgments**

790 S. Romano has carried out this work with the support of a postdoctoral fellowship from the Consorzio
791 Nazionale Interuniversitario per le Scienze fisiche della Materia (CNISM). The financial support of
792 EARLINET as part of the ACTRIS Research Infrastructure Project by the European Union's Horizon
793 2020 research and innovation programme under grant agreement no. 654169 (previously under grant
794 agreement no. 262254) in the 7th Framework Programme (FP7/2007-2013) is gratefully
795 acknowledged. The NOAA Air Resources Laboratory is kindly acknowledged for the provision of
796 the HYSPLIT back trajectories.

798 **References**

799

800 Bardouki, H., Liakakou, H., Economou, C., Sciare, J., Smolík, J., Ždímal, V., Eleftheriadis, K.,
801 Lazaridis, M., Dye, C., Mihalopoulos, N., 2003. Chemical composition of size-resolved
802 atmospheric aerosols in the eastern Mediterranean during summer and winter. Atmos. Environ.
803 37, 195-208. DOI: 10.1016/S1352-2310(02)00859-2.

804 Barmet, P., Kuster, T., Muhlbauer, A., Lohmann, U., 2009. Weekly cycle in particulate matter versus
805 weekly cycle in precipitation over Switzerland. J. Geophys. Res. 114, D05206. DOI: 10.1029/2008
806 JD011192.

807 Barmpadimos, I., Nufer, M., Oderbolz, D.C., Keller, J., Aksoyoglu, S., Hueglin, C., Baltensperger,
808 U., Prévôt, A.S.H., 2011. The weekly cycle of ambient concentrations and traffic emissions of
809 coarse (PM10 - PM2.5) atmospheric particles. Atmos. Environ. 45, 4580-4590. DOI: 10.1016/j.
810 atmosenv.2011.05.068.

811 Baró, R., Lorente-Plazas, R., Jerez, S., Montávez, J.P., Jiménez-Guerrero, P., 2015. Are atmospheric
812 aerosols able to modify the surface winds? A sensitivity study of the biomass burning aerosols
813 impact on the spatially-distributed wind over Europe. Geophys. Res. Abstracts 17, EGU2015-
814 8963.

815 Bäumer, D., Rinke, R., Vogel, B., 2008. Weekly periodicities of Aerosol Optical Thickness over
816 Central Europe – evidence of an anthropogenic direct aerosol effect. Atmos. Chem. Phys. 8, 83-
817 90. DOI: 10.5194/acp-8-83-2008.

818 Belis, C.A., Larsen, B.R., Amato, F., El Haddad, I., Favez, O., Harrison, R.M., Hopke, P.K., Nava,
819 S., Paatero, P., Prevot, A., Quass, U., Vecchi, R., Viana, M., 2014. European Guide on Air
820 Pollution Source Apportionment with Receptor Models. Report EUR 26080 EN. Luxembourg:
821 Publication Office of the European Union, 88 pp. ISBN: 978-92-79-32514-4.

822 Bernardoni, V., Vecchi, R., Valli, G., Piazzalunga, A., Fermo, P., 2011. PM10 source apportionment
823 in Milan (Italy) using time-resolved data. Sci. Total Environ. 409, 4788-4795. DOI:
824 10.1016/j.scitotenv.2011.07.048.

825 Bigi, A., Ghermandi, G., 2016. Trends and variability of atmospheric PM2.5 and PM10-2.5
826 concentration in the Po Valley, Italy. Atmos. Chem. Phys. 16, 15777-15788. DOI: 10.5194/acp-
827 16-15777-2016.

828 Birch, M.E., Cary, R.A., 1996. Elemental Carbon-Based Method for Monitoring Occupational
829 Exposures to Particulate Diesel Exhaust. Aerosol Sci. Technol. 25, 221-241. DOI: 10.1080/
830 02786829608965393.

831 Becagli, S., Sferlazzo, D.M., Pace, G., di Sarra, A., Bommarito, C., Calzolai, G., Ghedini, C.,
832 Lucarelli, F., Meloni, D., Monteleone, F., Severi, M., Traversi, R., Udisti, R., 2012. Evidence for
833 heavy fuel oil combustion aerosols from chemical analyses at the island of Lampedusa: a possible
834 large role of ships emissions in the Mediterranean. Atmos. Chem. Phys. 12, 3479-3492. DOI:
835 10.5194/acp-12-3479-2012.

836 Bove, M.C., Brotto, P., Calzolai, G., Cassola, F., Cavalli, F., Fermo, P., Hjorth, J., Massabò, D., Nava,
837 S., Piazzalunga, A., Schembari, C., Prati, P., 2016. PM10 source apportionment applying PMF
838 and chemical tracer analysis to ship-borne measurements in the Western Mediterranean. Atmos.
839 Environ. 125, 140-151. DOI: 10.1016/j.atmosenv.2015.11.0091352-2310.

840 Calzolai, G., Nava, S., Lucarelli, F., Chiari, M., Giannoni, M., Becagli, S., Traversi, R., Marconi, M.,
841 Frosini, D., Severi, M., Udisti, R., di Sarra, A., Pace, G., Meloni, D., Bommarito, C., Monteleone,
842 F., Anello, F., Sferlazzo, D.M., 2015. Characterization of PM10 sources in the central Medi-
843 terranean. Atmos. Chem. Phys. 15, 13939-13955. DOI: 10.5194/acp-15-13939-2015.

844 Cesari, D., Genga, A., Ielpo, P., Siciliano, M., Mascolo, G., Grasso, F.M., Contini, D., 2014. Source
845 apportionment of PM2.5 in the harbour–industrial area of Brindisi (Italy): Identification and

846 estimation of the contribution of in-port ship emissions. Sci. Total Environ. 497-498, 392-400.
847 DOI: 10.1016/j.scitotenv.2014.08.007.

848 Danalatos, D., Glavas, S., 1999. Gas phase nitric acid, ammonia and related particulate matter at a
849 Mediterranean coastal site, Patras, Greece. Atmos. Environ. 33, 3417-3425. DOI: 10.1016/S1352-
850 2310(98)00342-2.

851 Draxler, R.R., Rolph, G.D., 2003. HYSPLIT (HYbrid Single-Particle Lagrangian Integrated
852 Trajectory) Model access via NOAA ARL READY Website (http://www.arl.noaa.gov/ready/
853 hysplit4.html), NOAA Air Resources Laboratory, Silver Spring, MD.

854 Georgoulias, A.K., Kourtidis, K.A., 2011. On the aerosol weekly cycle spatiotemporal variability
855 over Europe. Atmos. Chem. Phys. 11, 4611-4632. DOI: 10.5194/acp-11-4611-2011.

856 Georgoulias, A.K., Kourtidis, K.A., 2012. A high resolution satellite view of the aerosol weekly cycle
857 variability over Central Europe. Atmos. Res. 107, 145-160. DOI: 10.1016/j.atmosres.2012.01.003.

858 Georgoulias, A.K., Kourtidis, K.A., Alexandri, G., Rapsomanikis, S., Sanchez-Lorenzo, A., 2015.
859 Common summertime total cloud cover and aerosol optical depth weekly variabilities over
860 Europe: Sign of the aerosol indirect effects? Atmos. Res. 153, 59-73. DOI: 10.1016/j.atmosres.
861 2014.07.031.

862 Gong, D.Y., Ho, C.H., Chen, D., Qian, Y., Choi, Y.S., Kim, J., 2007. Weekly cycle of
863 aerosol-meteorology interaction over China. J. Geophys. Res. 112, D22202. DOI: 10.1029/2007JD
864 008888.

865 Hayn, M., Beirle, S., Hamprecht, F.A., Platt, U., Menze, B.H., Wagner, T., 2009. Analysing spatio-
866 temporal patterns of the global NO2-distribution retrieved from GOME satellite observations
867 using a generalized additive model. Atmos. Chem. Phys. 9, 6459-6477. DOI: 10.5194/acp-9-6459-
868 2009.

869 Hendricks Franssen, H.-J., 2008. Comment on "An unexpected pattern of distinct weekly periodicities
870 in climatological variables in Germany" by Dominique Bäumer and Bernhard Vogel. Geophys.
871 Res. Lett. 35, L05802. DOI: 10.1029/2007GL031279.

872 Jacobson, M.Z., 1998. Studying the effects of aerosols on vertical photolysis rate coefficient and
873 temperature profiles over an urban airshed. J. Geophys. Res. 103, 10593-10604. DOI: 10.1029
874 /98JD00287.

875 Jacobson, M.Z., Kaufman, Y.J., 2006. Wind reduction by aerosol particles. Geophys. Res. Lett. 33,
876 L24814. DOI: 10.1029/2006GL027838.

877 Kerminen, V.M., Aurela, M., Hillamo, R.E., Virkkula, A., 1997. Formation of particulate MSA:
878 deductions from size distribution measurements in the Finnish Arctic. Tellus B 49(2), 159-171.
879 DOI: 10.1034/j.1600-0889.49.issue2.4.x.

880 Koçak, M., Mihalopoulos, N., Kubilay, N., 2007. Chemical Composition of the Fine and Coarse
881 Fraction of Aerosols in the Northeastern Mediterranean. Atmos. Environ. 41, 7351-7368. DOI:
882 10.1016/j.atmosenv.2007.05.011.

883 Lelieveld, J., Berresheim, H., Borrmann, S., Crutzen, P.J., Dentener, F.J., Fischer, H., Feichter, J.,
884 Flatau, P.J., Heland, J., Holzinger, R., Korrmann, R., Lawrence, M.G., Levin, Z., Markowicz,
885 K.M., Mihalopoulos, N., Minikin, A., Ramanathan, V., de Reus, M., Roelofs, G.J., Scheeren, H.A.,
886 Sciare, J., Schlager, H., Schultz, M., Siegmund, P., Steil, B., Stephanou, E.G., Stier, P., Traub, M.,
887 Warneke, C., Williams, J., Ziereis, H., 2002. Global air pollution crossroads over the
888 Mediterranean. Science 298, 794-799. DOI: 10.1126/science.1075457.

889 Li, M., Wang, T., Xie, M., Zhuang, B., Li, S., Han, Y., Chen, P., 2017. Impacts of aerosol-radiation
890 feedback on local air quality during a severe haze episode in Nanjing megacity, eastern China.
891 Tellus B 69 (1). DOI: 10.1080/16000889.2017.1339548.

892 Liu, J., Li, J., Li, W., 2016. Temporal Patterns in Fine Particulate Matter Time Series in Beijing: A
893 Calendar View. Sci. Rep. 6, 32221. DOI: 10.1038/srep32221.

894 Mazzei, F., D'Alessandro, A., Lucarelli, F., Marenco, F., Nava, S., Prati, P., Valli, G., Vecchi, R.,
895 2006. Elemental composition and source apportionment of particulate matter near a steel plant in
896 Genoa (Italy). Nucl. Instrum. Methods Phys. Res. B: Beam Interact. Mater. Atoms 249, 548-551.
897 DOI: 10.1016/j.nimb.2006.03.050.

898 Miyakawa, T., Takegawa, N., Kondo, Y., 2007. Removal of sulfur dioxide and formation of sulfate
899 aerosol in Tokyo. J. Geophys. Res. 112, D13209. DOI: 10.1029/2006JD007896.

900 Morganti, A., Becagli, S., Castellano, E., Severi, M., Traversi, R., Udisti, R., 2007. An improved flow
901 analysis-ion chromatography method for determination of cationic and anionic species at trace
902 levels in Antarctic ice cores. Anal. Chim. Acta 603, 190-198. DOI: 10.1016/j.aca.2007.09.050.

903 Nicolas, J.F., Galindo, N., Yubero, E., Pastor, C., Esclapez, R., Crespo, J., 2009. Aerosol Inorganic
904 Ions in a Semiarid Region on the Southeastern Spanish Mediterranean Coast. Water Air Soil
905 Pollut. 201, 149-159. DOI: 10.1007/s11270-008-9934-2.

906 NIOSH, 1999. Method 5040 Issue 3 (Interim): Elemental Carbon (Diesel Exhaust). In NIOSH
907 Manual of Analytical Methods. National Institute of Occupational Safety and Health, Cincinnati,
908 OH.

909 Norris, G., Duvall, R., Brown, S., Bai, S., 2014. EPA Positive Matrix Factorization (PMF) 5.0
910 fundamentals and user guide. Prepared for the U.S. Environmental Protection Agency Office of
911 Research and Development, Washington, DC, EPA/600/R-14/108.

912 Paatero, P., 2000. User's Guide for the Multilinear Engine Program “ME2” for Fitting Multilinear
913 and Quasi-multilinear Models (February).

914 Paatero, P., 2015. User’s Guide for Positive Matrix Factorization Programs PMF2 and PMF3, Part 1-
915 2: Tutorial. University of Helsinki: Helsinki, Finland (update 31 March 2015).

916 Paatero, P., Tapper, U., 1994. Positive matrix factorization: A non-negative factor model with optimal
917 utilization of error estimates of data values. Environmetrics 5, 111-126. DOI:10.1002/env.
918 3170050203.

919 Perrone, M.R., Carofalo, I., Dinoi, A., Buccolieri, A., Buccolieri, G., 2009. Ionic and elemental
920 composition of TSP, PM10, and PM2.5 samples collected over South-East Italy. Il Nuovo Cimento
921 B 124, 341-356. DOI: 10.1393/ncb/i2009-10770-2.

922 Perrone, M.R., Piazzalunga, A., Prato, M., Carofalo, I., 2011. Composition of fine and coarse particles
923 in a coastal site of the central Mediterranean: Carbonaceous species contributions. Atmos.
924 Environ. 45(39), 7470-7477. DOI: 10.1016/j.atmosenv.2011.04.030.

925 Perrone, M.R., Becagli, S., Garcia Orza, J.A.G., Vecchi, R., Dinoi, A., Udisti, R., Cabello, M., 2013.
926 The impact of long-range-transport on PM1 and PM2.5 at a Central Mediterranean site. Atmos.
927 Environ. 71, 176-186. DOI: 10.1016/j.atmosenv.2013.02.006.

928 Perrone, M.R., Dinoi, A., Becagli, S., Udisti, R., 2014. Chemical composition of PM1 and PM2.5 at
929 a suburban site in southern Italy. Int. J. Environ. An. Ch. 94, 127-150. DOI: 10.1080/03067319.
930 2013.791978.

931 Perrone, M.R., Romano, S., Orza, J.A.G., 2015. Columnar and ground-level aerosol optical
932 properties: sensitivity to the transboundary pollution, daily and weekly patterns, and relationships.
933 Environ. Sci. Pollut. R. 22, 16570-16589. DOI: 10.1007/s11356-015-4850-7.

934 Perrone, M.R., Genga, A., Siciliano, M., Siciliano, T., Paladini, F., Burlizzi, P., 2016. Saharan dust
935 impact on the chemical composition of PM10 and PM1 samples over south-eastern Italy. Arab. J.
936 Geosci. 9, 127. DOI: 10.1007/s12517-015-2227-3.

937 Perrone, M.R., Romano, S., 2018. Relationship between the planetary boundary layer height and the
938 particle scattering coefficient at the surface. Atmos. Res. 213, 57-69. DOI: 10.1016/j.atmosres.
939 2018.04.017.

940 Pey, J., Querol, X., Alastuey, A., 2009. Variations of levels and composition of PM10 and PM2.5 at
941 an insular site in the Western Mediterranean. Atmos. Res. 94, 285-299. DOI: 10.1016/j.atmosres.
942 2009.06.006.

943 Pietrogrande, M.C., Manarini, F., Perrone, M.R., Udisti, R., Romano, S., Becagli, S., 2018. PM10
944 Oxidative Potential at a Central Mediterranean Site: Association with Chemical Composition and
945 Meteorological Parameters. Atmos. Environ. 188, 97-111. DOI: 10.1016/j.atmosenv.2018.06.013.

946 Polissar, A.V., Hopke, P.K., Paatero, P., Malm, W.C., Sisler, J.F., 1998. Atmospheric Aerosol over
947 Alaska: 2. Elemental Composition and Sources. J. Geophys. Res. 103, 19045-19057. DOI:
948 10.1029/98JD01212.

949 Putaud, J.P., Van Dingenen, R., Alastuey, A., Bauer, H., Birmili, W., Cyrys, J., Flentje, H., Fuzzi, S.,
950 Gehrig, R., Hansson, H.C., Harrison, R.M., Herrmann, H., Hitzenberger, R., Huglin, C., Jones, A.
951 M., Kasper-Giebl, A., Kiss, G., Kousa, A., Kuhlbusch, T.A.J., Loschau, G., Maenhaut, W.,
952 Molnar, A., Moreno, T., Pekkanen, J., Perrino, C., Pitz, M., Puxbaum, H., Querol, X., Rodriguez,
953 S., Salma, I., Schwarz, J., Smolik, J., Schneider, J., Spindler, G., ten Brink, H., Tursic, J., Viana,
954 M., Wiedensohler, A., Raes, F., 2010. A European aerosol phenomenology – 3: Physical and
955 chemical characteristics of particulate matter from 60 rural, urban, and kerbside sites across
956 Europe. Atmos. Environ. 44, 1308-1320. DOI: 10.1016/j.atmosenv.2009.12.011.

957 Quaas, J., Boucher, O., Jones, A., Weedon, G.P., Kieser, J., Joos, H., 2009. Exploiting the weekly
958 cycle as observed over Europe to analyse aerosol indirect effects in two climate models. Atmos.
959 Chem. Phys. 9, 8493-8501. DOI: 10.5194/acp-9-8493-2009.

960 Querol, X., Pey, J., Minguillón, M.C., Pérez, N., Alastuey, A., Viana, M., Moreno, T., Bernabé, R.
961 M., Blanco, S., Cárdenas, B., Vega, E., Sosa, G., Escalona, S., Ruiz, H., Artíñano, B., 2008. PM
962 speciation and sources in Mexico during the MILAGRO-2006 Campaign. Atmos. Chem. Phys. 8,
963 111-128. DOI: 10.5194/acp-8-111-2008.

964 Querol, X., Alastuey, A., Pey, J., Cusack, M., Pérez, N., Mihalopoulos, N., Theodosi, C.,
965 Gerasopoulos, E., Kubilay, N., Koçak, M., 2009. Variability in regional background aerosols
966 within the Mediterranean. Atmos. Chem. Phys. 9, 4575-4591. DOI: 10.5194/acp-9-4575-2009.

967 Romano, S., Lo Feudo, T., Calidonna, C.R., Burlizzi, P., Perrone, M.R., 2017. Solar eclipse of 20
968 March 2015 and impacts on irradiance, meteorological parameters, and aerosol properties over
969 southern Italy. Atmos. Res. 198, 11-21. DOI: 10.1016/j.atmosres.2017.08.001.

970 Romano, S., Burlizzi, P., Kinne, S., De Tomasi, F., Hamann, U., Perrone, M.R., 2018. Radiative
971 impact of Etna volcanic aerosols over south eastern Italy on 3 December 2015. Atmos. Environ.
972 182, 155-170. DOI: 10.1016/j.atmosenv.2018.03.038.

973 Rosenfeld, D., Lohman, U., Raga, G.B., O'Dowd, C.D., Kulmala, M., Fuzzi, S., Reissell, A.,
974 Andreae, M.O., 2008. Flood or drought: How do aerosols affect precipitation? Science 321, 1309-
975 1313. DOI: 10.1126/science.1160606.

976 Sanchez-Lorenzo, A., Calbó, J., Martin-Vide, J., Garcia-Manuel, A., García-Soriano, G., Beck, C.,
977 2008. Winter "weekend effect" in southern Europe and its connections with periodicities in
978 atmospheric dynamics. Geophys. Res. Lett. 35, L15711. DOI: 10.1029/2008GL034160.

979 Sanchez-Lorenzo, A., Laux, P., Hendricks Franssen H.-J., Calbó, J., Vogl, S., Georgoulias, A.K.,
980 Quaas, J., 2012. Assessing large-scale weekly cycles in meteorological variables: a review. Atmos.
981 Chem. Phys. 12, 5755-5771. DOI: 10.5194/acp-12-5755-2012.

982 Schultz, D.M., Mikkonen, S., Laaksonen, A., Richman, M.B., 2007. Weekly precipitation cycles?
983 Lack of evidence from United States surface stations. Geophys. Res. Lett. 34, L22815. DOI:
984 10.1029/2007GL031889.

985 Seinfeld, J.H., Pandis, S.N., 1998. Atmospheric Chemistry and Physics: From Air Pollution to
986 Climate Change. J. Wiley &Sons, INC.

987 SPECIEUROPE Source profiles for Europe database, Joint Research Centre, Ispra

http://source-apportionment.jrc.ec.europa.eu/Specieurope/index.aspx.

Srimuruganandam, B., Nagendra, S., Madanayak, S., 2010. Analysis and interpretation of particulate matter – PM10, PM2.5 and PM1 emissions from the heterogeneous traffic near an urban roadway. Atmos. Pollut. Res. 1, 184-194. DOI: 10.5094/APR.2010.024.

Stern, A.C., 1977. Air pollution. Academic Press Inc., Harcourt Brace Jovanovich Press, Vol. I-VIII.I.

Stjern, C.W., 2011. Weekly cycles in precipitation and other meteorological variables in a polluted region of Europe. Atmos. Chem. Phys. 11, 4095-4104. DOI: 10.5194/acp-11-4095-2011.

Taiwo, A.M., Beddows, D.C., Calzolai, G., Harrison, R.M., Lucarelli, F., Nava, S., Shi, Z., Valli, G., Vecchi, R., 2014. Receptor modelling of airborne particulate matter in the vicinity of a major steelworks site. Sci. Total Environ. 490, 488-500. DOI: 10.1016/j.scitotenv.2014.04.118.

Vecchi, R., Bernardoni, V., Fermo, P., Lucarelli, F., Mazzei, F., Nava, S., Prati, P., Piazzalunga, A., Valli, G., 2009. 4-hours resolution data to study PM10 in a "hot spot" area in Europe. Environ. Monit. Assess. 154, 283-300. DOI: 10.1007/s10661-008-0396-1.

Vecchi, R., Bernardoni, V., Valentini, S., Piazzalunga, S., Fermo, P., Valli, G., 2018. Assessment of light extinction at a European polluted urban area during wintertime: Impact of PM1 composition and sources. Env. Pollut. 233, 679-689. DOI: 10.1016/j.envpol.2017.10.059.

Viana, M., Querol, X., Alastuey, A., 2006. Chemical characterisation of PM episodes in NE Spain. Chemosphere 62/6, 947-956. DOI: 10.1016/j.chemosphere.2005.05.048.

Wagstrom, K.M., Pandis, S.N., 2009. Determination of the age distribution of primary and secondary aerosol species using a chemical transport model. J. Geophys. Res. 114, D14303. DOI: 10.1029/2009JD011784.

Xia, X., Eck, T.F., Holben, B.N., Phillippe, G., Chen, H., 2008. Analysis of the weekly cycle of aerosol optical depth using AERONET and MODIS data. J. Geophys. Res. 113, D14217. DOI: 10.1029/2007JD009604.

SUPPLEMENTARY MATERIAL

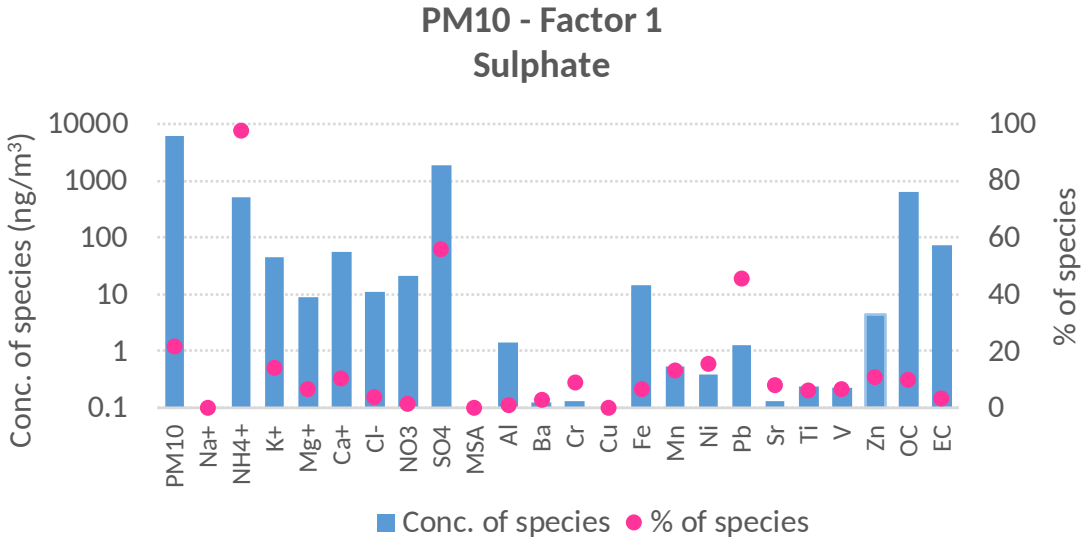

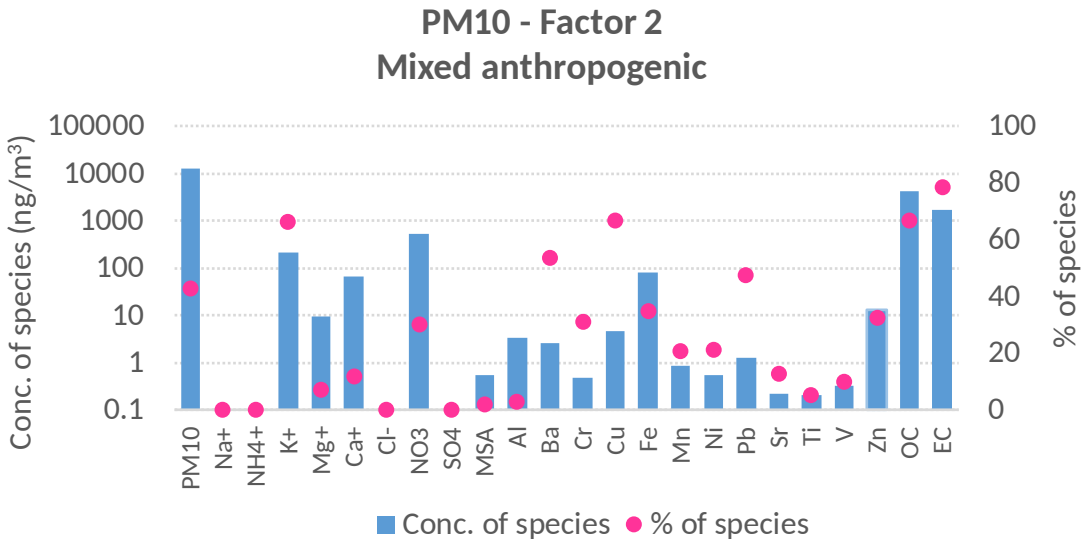

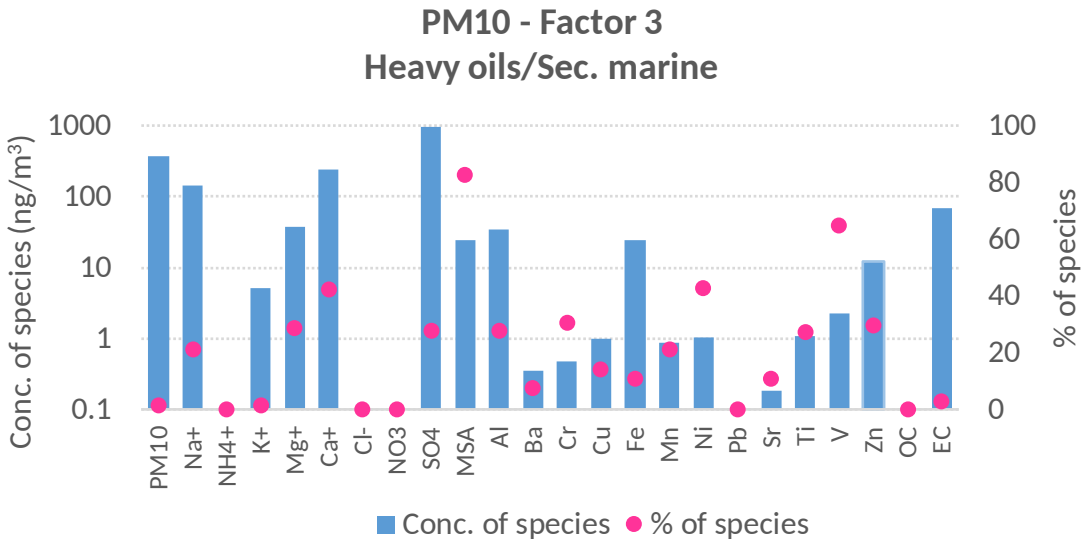

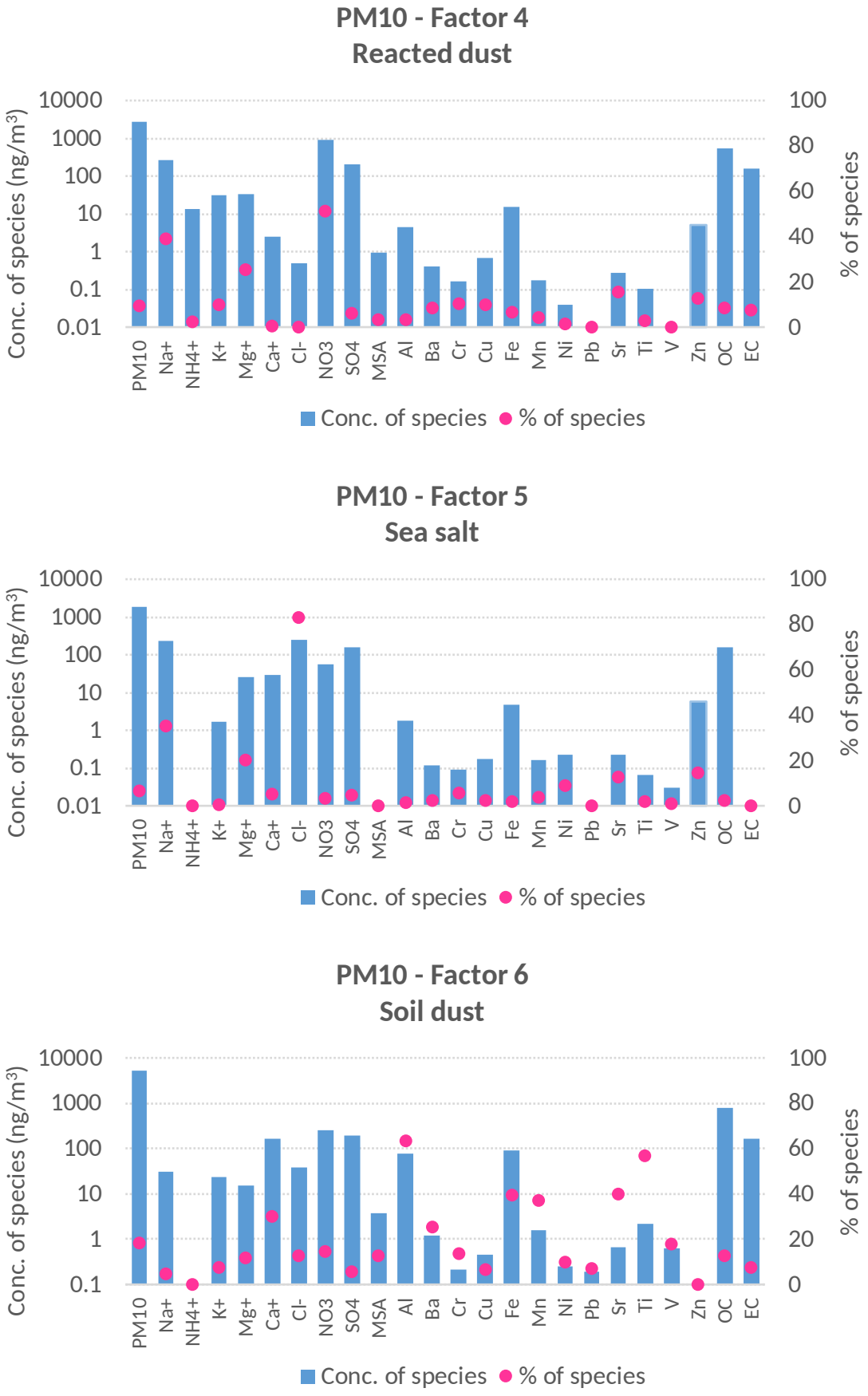

Figure S1. Chemical profiles and percentage contributions of the six PMF factors identified by PMF in PM10.

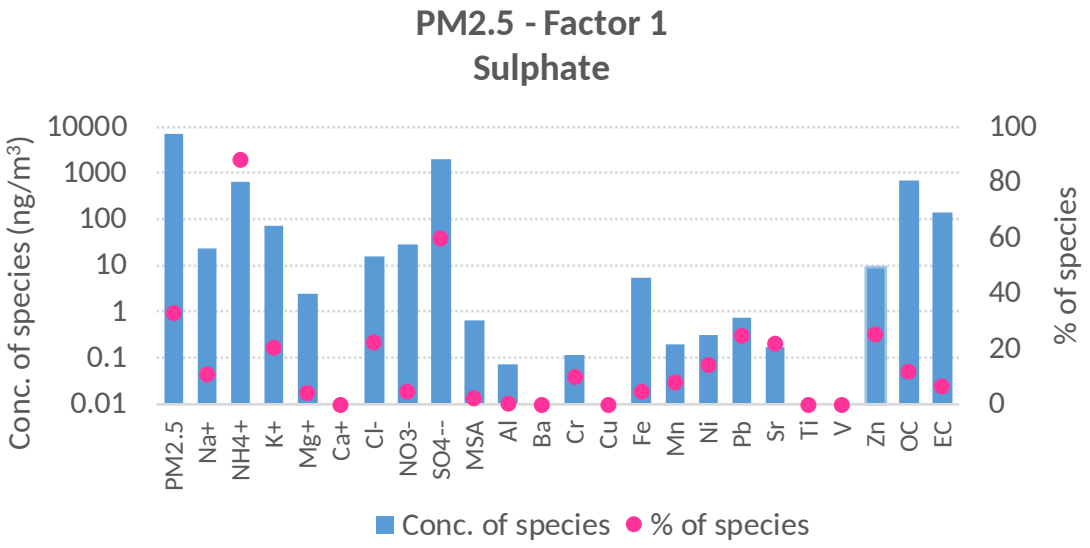
PM2.5 - Factor 1
Sulphate
Conc. of species (ng/m³)
% of species
10000
1000
100
10
1
0.1
0.01
100
80
60
40
20
0
PM2.5
Na+
NH4+
K+
Mg+
Ca+
Cl-
NO3-
SO4--
MSA
Al
Ba
Cr
Cu
Fe
Mn
Ni
Pb
Sr
Ti
V
Zn
OC
EC
Conc. of species
% of species

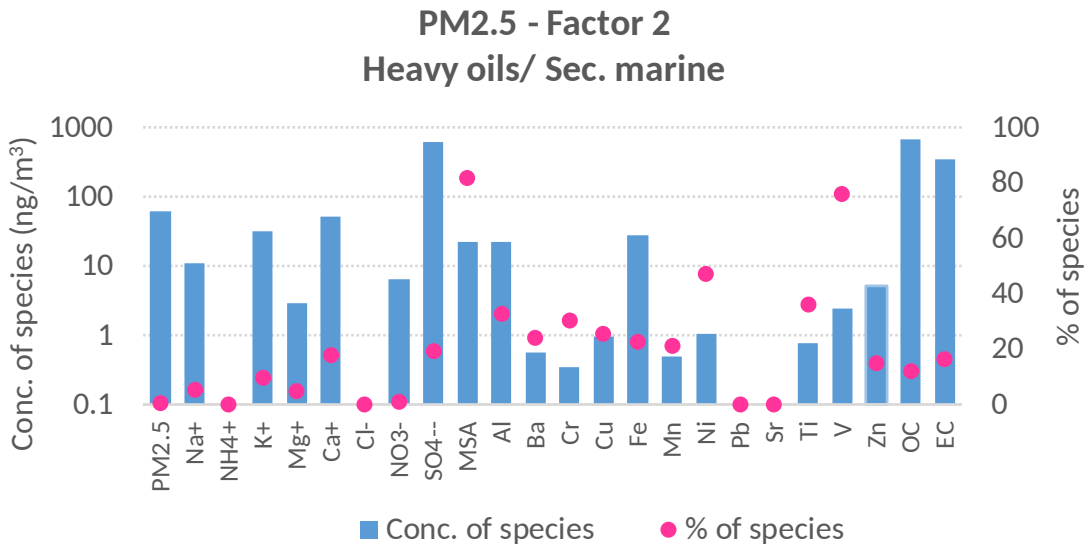
PM2.5 - Factor 2
Heavy oils/ Sec. marine
Conc. of species (ng/m³)
% of species
1000
100
10
1
0.1
100
80
60
40
20
0
PM2.5
Na+
NH4+
K+
Mg+
Ca+
Cl-
NO3-
SO4--
MSA
Al
Ba
Cr
Cu
Fe
Mn
Ni
Pb
Sr
Ti
V
Zn
OC
EC
Conc. of species
% of species

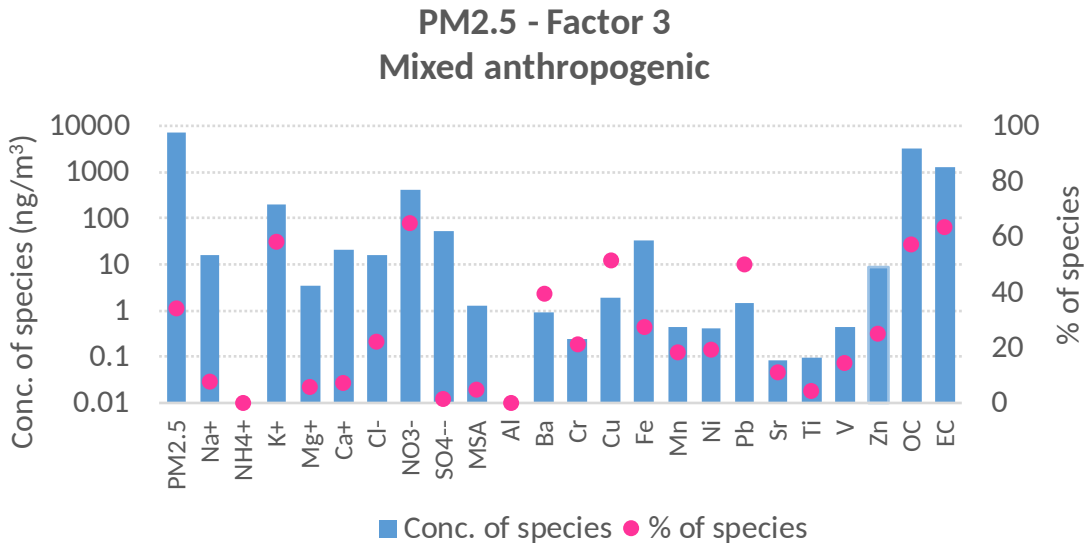
PM2.5 - Factor 3
Mixed anthropogenic
Conc. of species (ng/m³)
% of species
10000
1000
100
10
1
0.1
0.01
100
80
60
40
20
0
PM2.5
Na+
NH4+
K+
Mg+
Ca+
Cl-
NO3-
SO4--
MSA
Al
Ba
Cr
Cu
Fe
Mn
Ni
Pb
Sr
Ti
V
Zn
OC
EC
Conc. of species
% of species

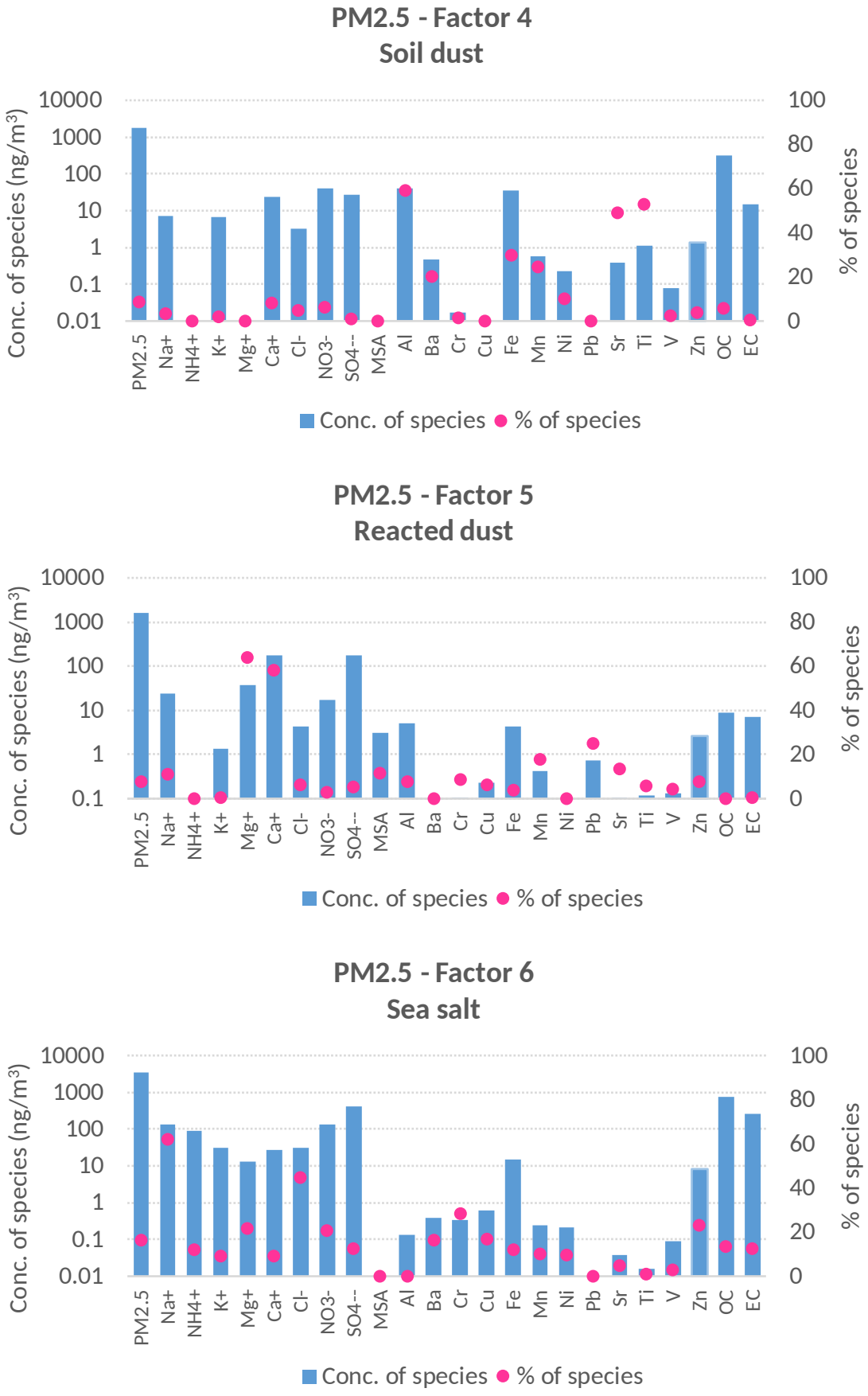

Figure S2. Chemical profiles and percentage contributions of the six PMF factors identified by PMF in PM2.5.

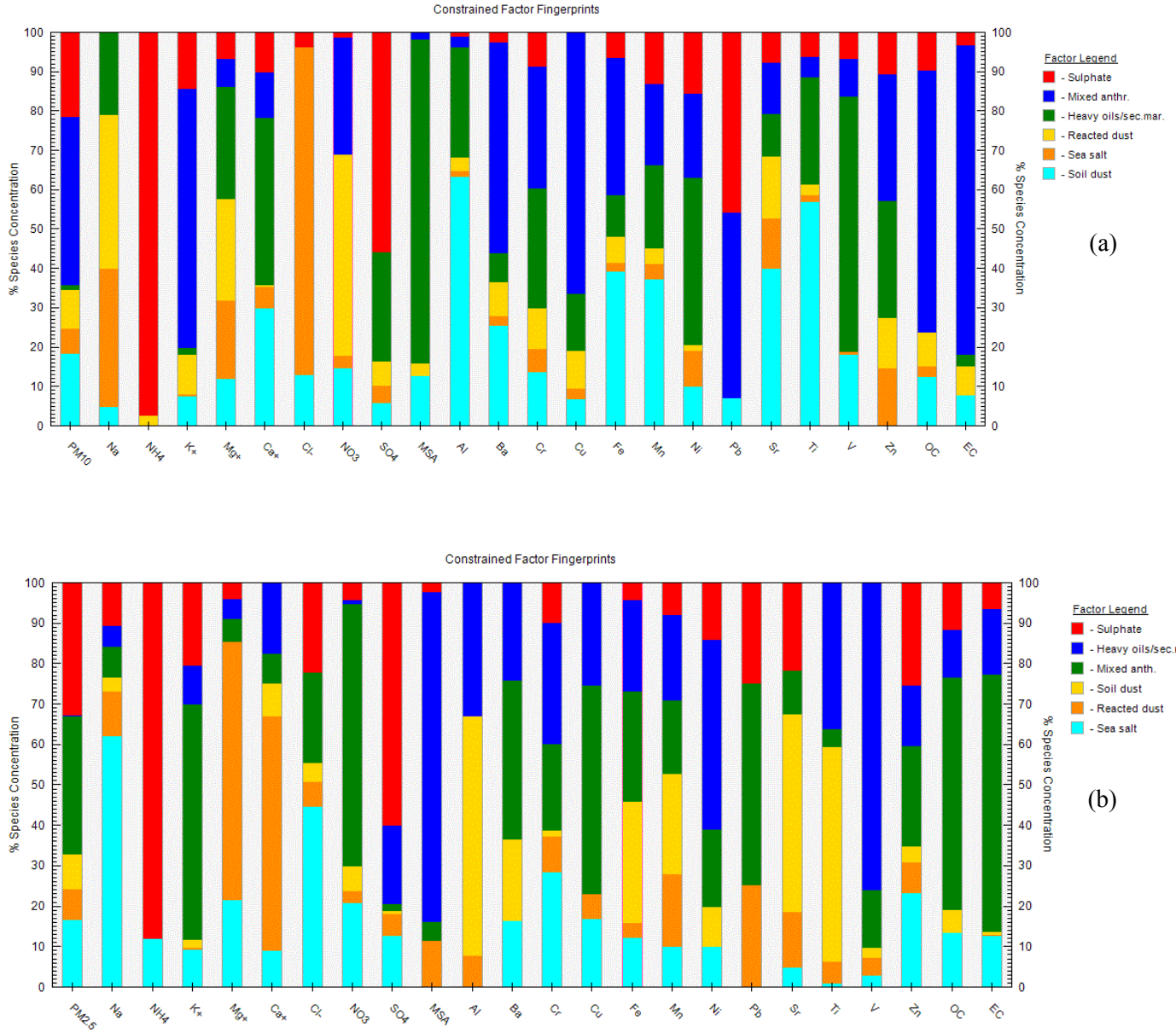

Figure S3. Percentage contributions of chemical components to the six identified aerosol sources of (a) PM10 and (b) PM2.5 particles.

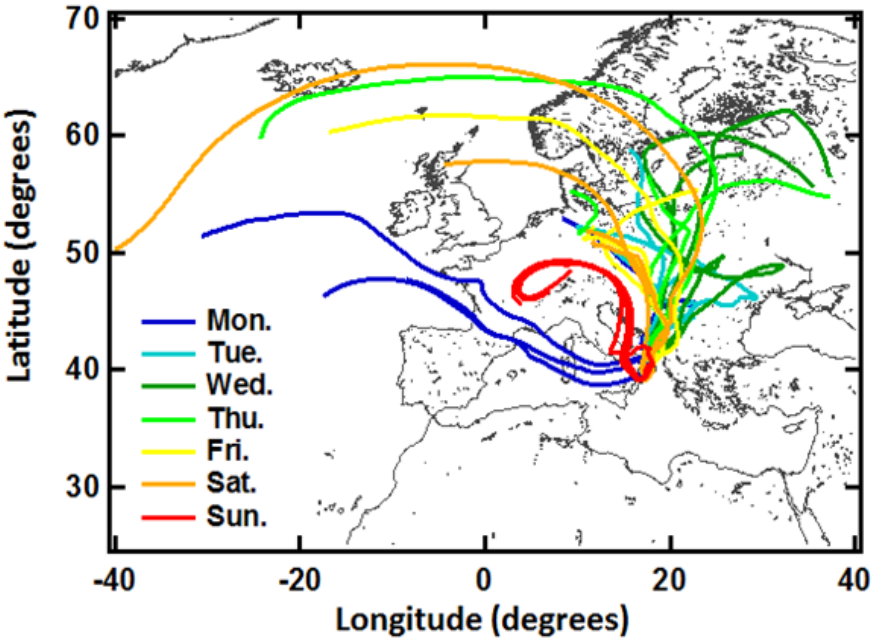

Figure S4. Pathways of the four-day back trajectories that reached the study site at 500 m above sea level, at 00:00, 06:00, 12:00, and 18:00 UTC for each day of the week April 6-12, 2015.

Table S1. Confidence level percentage of the difference between the Thursday and the Sunday average percent departure (APD) value of each analyzed chemical compound (Na^+, $NH4^+$, K^+, Ca^{2+}, NO_3^-, SO_4^{2-}, OC, and EC) in Autumn-Winter (AW) and in Spring-Summer (SS) and for PM10 and PM2.5, calculated by the two-tailed t-test and the Kruskal-Wallis (KW) test.

Chemical Compound	PM Fraction	Season	Confidence Level (%)	
			T-TEST	KRUSKAL-WALLIS TEST
Na^+	PM10	AW	33	30
		SS	62	62
	PM2.5	AW	25	18
		SS	88	84
NH_4^+	PM10	AW	88	76
		SS	92	84
	PM2.5	AW	89	87
		SS	94	97
K^+	PM10	AW	5	18
		SS	92	79
	PM2.5	AW	6	6
		SS	88	79
Ca^{2+}	PM10	AW	93	96
		SS	99	99
	PM2.5	AW	99	99
		SS	88	93
NO_3^-	PM10	AW	63	61
		SS	80	84
	PM2.5	AW	66	76
		SS	17	5
SO_4^{2-}	PM10	AW	87	96
		SS	17	10
	PM2.5	AW	87	81
		SS	42	54
OC	PM10	AW	57	34
		SS	80	71
	PM2.5	AW	59	46
		SS	69	38
EC	PM10	AW	25	7
		SS	70	55
	PM2.5	AW	28	7
		SS	58	47